FOILING SuMoth CHALLENGE

POLIMI
SAILING TEAM

POLITECNICO
MILANO 1863

Foiling SuMoth Challenge Stage 1 - 2024

DESIGN, MANUFACTURING & SUSTAINABILITY

sponsored by

11TH HOUR RACING

MARINESHIFT360

PERSICO

Bcomp

POLIMI SAILING TEAM | POLITECNICO DI MILANO, MILAN, ITALY | polimisailingteam@gmail.com

Abstract

The 2024 SuMoth project focuses on enhancing our existing prototype, Febe, by integrating sustainable solutions and advanced engineering innovations. This year's upgrades reflect our commitment to environmental sustainability and high-performance design. We have redesigned the deck cover for better aerodynamics, reconstructed the wings with recyclable materials, and optimized the rudder and main foil for improved durability and reduced drag. Our team has also designed a state-of-the-art mechatronic system, featuring a central onboard computer connected to a range of sensors, enabling precise control and enhanced performance. The introduction of new fly-by-wire systems, innovative lamination techniques, and advanced control algorithms highlight our dedication to cutting-edge technology. Through these comprehensive upgrades, Febe now boasts improved performance, stability, and sustainability. The 2024 SuMoth project showcases the ingenuity and hard work of our team, pushing the boundaries of sustainable design while adhering to eco-friendly practices.

Introduction

In the 2023-2024 season, the PoliMi Sailing Team has continued to push the boundaries of innovation and performance with our prototype, Febe. Building on last year's achievements and lessons, this year has been about refining and enhancing every aspect of the boat to ensure it surpasses our high expectations. Our engineering and design team kicked off the season with a deep dive into optimizing Febe's aerodynamic and hydrodynamic properties. The focus was put on the deck cover, implementing vortex generators and fine-tuning its dimensions to reduce drag. Using advanced Computational Fluid Dynamics (CFD) simulations, a smoother airflow was achieved and hydrodynamic drag was minimized: this translates to better overall performance on the water. The wings had been redesigned using recyclable materials, creating a sandwich structure that boosts flexural stiffness without adding weight. Through rigorous Finite Element Method (FEM) analyses, the lamination sequences was perfected for the crossbars and trampolines, ensuring they are not only stronger but also more environmentally friendly than last year's versions. The gantry has also seen a transformative redesign aimed at reducing drag and improving takeoff performance: Two innovative gantry designs were explored, utilizing cutting-edge composite materials and 3D printing technologies. These new designs maintain the necessary mechanical strength while keeping the structure lightweight. Hydrodynamic optimization was a major focus this year. An adjoint-based shape optimization was adopted for the main foil and rudder, significantly reducing drag and enhancing efficiency. The introduction of a Particle Swarm Optimization algorithm helped achieving a 5% reduction in the drag coefficient for the new foil design, which was further validated through CFD analyses. Additionally, a comprehensive study on foil performance under ventilation conditions has been conducted in order to better understand and mitigate potential performance losses at high speeds. In the realm of mechatronics, an advanced control systems has been designed to make Febe even more responsive and stable. A sophisticated network of sensors, including IMUs, GPS, and ultrasonic sensors, was thought to provide real-time data for state estimation and control. The central onboard computer, running the Robot Operating System (ROS), ensures seamless communication and control of these sensors. The control algorithms were refined with a Kalman filter for sensor fusion. Sustainability has been at the heart of the design. The use of sustainable materials has been prioritized, such as basalt fiber and recycled PET core, and environmentally friendly production methods like vacuum infusion have been employed, without the direct use of mouldss. This kind of practices, combined with the reusing of existing components has further minimized the environmental footprint of the prototype, reflecting the commitment to sustainable innovation. Overall, this season has been about fine-tuning and perfecting Febe. With meticulous engineering, advanced computational analyses, and a steadfast commitment to sustainability, the PoliMi Sailing Team has raised the bar, setting new standards for excellence in the SuMoth Challenge.

Contents

List of Tables

List of Figures

1 ENGINEERING AND DESIGN

1.1 Deck cover

In pursuit of optimizing the aerodynamic performance of the SuMoth, a comprehensive study focusing on enhancing the design of the deck cover was conducted. The primary objective was to minimize drag while ensuring effective coverage of all control systems situated on the deck. The study was divided into two key areas: determining optimal length and height for full deck cover and investigating the potential of vortex generators to further enhance aerodynamic efficiency. A further development from last year's deck cover consisted in an experimental 3D printed mould, developed in collaboration with Wasp [18] with the idea of scaling up this process in the future.

1.1.1 Length and Height of Deck Cover

One of the critical aspects addressed in the study was to redesign the deck cover to adequately cover all control systems on the deck. Through analysis and simulations, it was determined that by extending the length and height strategically all components of the boat's control systems on the deck were adequately shielded, while maintaining smooth airflow around the boat in order to achieve optimal coverage without compromising aerodynamic performance.

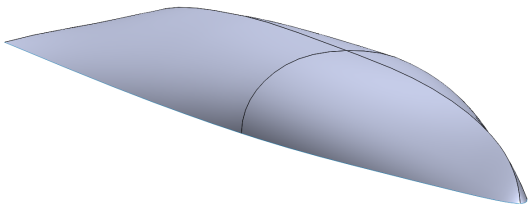

Figure 1.1: "Pointed" deck cover

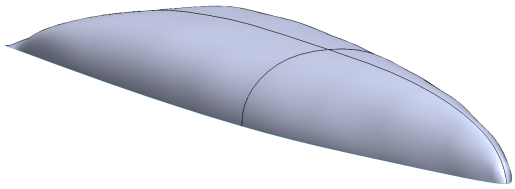

Figure 1.2: "Flat" deck cover

1.1.2 Fairing study

In addition to optimizing the dimensions of the deck cover, the study delved into the effectiveness of incorporating a vortex generator to further reduce drag. Vortex generators are small devices that manipulate airflow in order to generate controlled turbulence and enhance aerodynamic efficiency. As part of this investigation, a deck cover design featuring a pointed upper surface resembling a continuous vortex generator was tested. However, this approach proved ineffective as it caused flow separation in areas where it was not advantageous, negating the benefits gained. Consequently, it became evident that a different approach was necessary to maintain efficient airflow around the deck cover.

"Pointed" deck cover	"Flat" deck cover
CD: 9.27×10^{-3}	CD: 8.41×10^{-3}

Table 1.1: Comparison between pointed and flat deck cover's drag coefficients

1.1.3 Findings and Results

Through computational fluid dynamics (CFD) simulations, various configurations of traditional vortex generators strategically placed along the surface of the deck cover were assessed. This

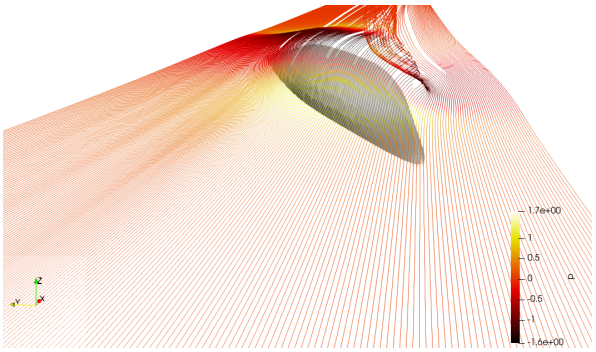

Figure 1.3: CFD on “Pointed” deck cover

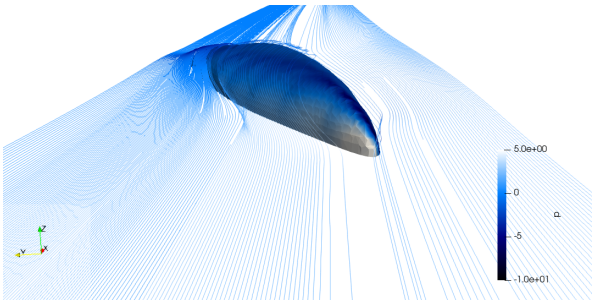

Figure 1.4: CFD on “Flat” deck cover

approach aimed to induce controlled vortices that would energize the boundary layer and reduce overall drag. The analysis indicated that these traditional vortex generators effectively minimize turbulence and drag without compromising the integrity of the airflow, thus demonstrating their suitability for optimizing the aerodynamic performance. The results of the study revealed promising outcomes: by adjusting the length and height of the windshield, a comprehensive coverage of the deck was achieved. Furthermore, the incorporation of vortex generators showed a significant reduction in turbulence and drag, enhancing the overall aerodynamic performance of the boat. In conclusion, the study on the new SuMoth deck cover has yielded valuable insights into optimizing aerodynamic efficiency while ensuring adequate coverage of deck control systems. By strategically adjusting the length and height and integrating vortex generators, it resulted in drag minimization and improved overall performance. These findings will not only enhance the competitiveness of our SuMoth boat but also contribute to advancements in aerodynamic design for similar watercraft in the future.

1.2 Wings

The main objectives of the project were to create a structure that could be produced without the use of mouldss and completely made of sustainable materials. In the preliminary phase of the design, it was decided to produce the wings in two components: the “Crossbars” and the “Trampolines”. Trampolines consist in two $1000mm$ x $1300mm$ x $5mm$ panels with longitudinal reinforcements; they are connected to the hull using the crossbars, diagonal elements with a $30°$ angle with a rectangular cross section whose height tapers from $55mm$ to $10mm$, in order to further reduce weight in the less stressed areas. Being both components mainly stressed through bending, a sandwich structure was chosen, so that the area moment of inertia of each section is increased (improving the flexural stiffness) without a significant weight increase.

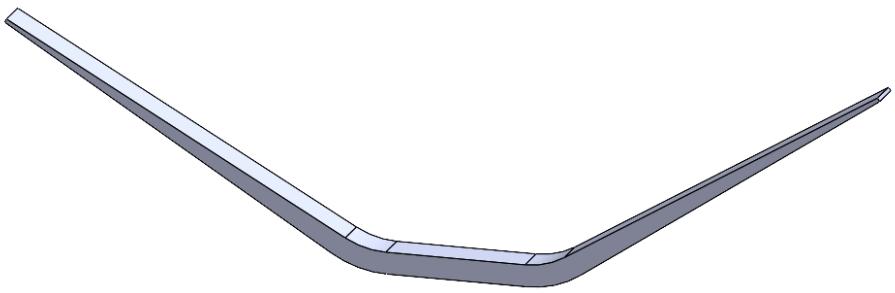

Figure 1.5: Crossbar

Several finite element models were created and assessed in order to have accurate results that reflect the real behavior of the manufactured wings and define the lamination sequence of each component. Initially, the two elements were analyzed separately and, at a later stage of the analysis, a full assembly model was developed to better investigate the behaviour of the

whole structure.

1.2.1 Crossbars FEM analysis

A mix of shell and solid elements was used to model the system: the former for the basalt skins, the latter for the PET core. This approach ensured very good reliability with a lower modelling effort than using solid elements only. To perform a static analysis, the chosen boundary condition was an *ENCASTRE* at the horizontal section representing the bonding connection to the hull. The loading condition represents the skipper sitting on the extremity of the wings: a downwards-facing force $F = 800N$ was applied in the direction normal to the inclined section. The materials used in the final configuration were unidirectional and woven basalt fibre fabrics and a Divinycell®[5]PR recycled PET core (made of up to 45% of post consumer PET) . Since the deformation is acceptable in the linear-elastic region only and considering the orthotropic properties of the fibers, the components were modeled as *lamina elastic* type for basalt fiber end *linear elastic* for PET. The main parameters accounted for in the results analysis were the maximum deformation (*Umax*) to be perceived by the skipper, *Tsai-Hill* failure criterion for the skins (where the intended maximum value was considered around 0.26 so to have a safety coefficient of 1.96) and *Tresca* equivalent stress for the core. This last criterion, even though normally used for ductile materials, was chosen because conservative, representing the maximum shear stress according to the Mohr theory. The lamination sequence was obtained after many different configurations in an iterative process that balances mechanical reliability, weight reduction, regulatory constraints, and external economic factors. The composite layup of the crossbars is divided in 5 different sections, 3 on the upper and lower surface and 2 on the lateral one, with a number of plies ranging from for 1 to 6, with the use of both unidirectional and twill fabrics. The behavior produced by these lamination sequences is shown in the figures below, where the trade-off between mechanical properties and the weight of the components shows a correct multi-objective optimization, achieving a strong bending stiffness while limiting the weight to $1.66Kg$.

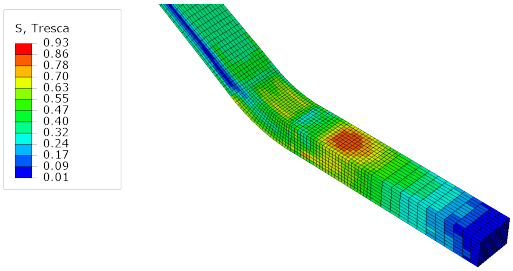

Figure 1.6: Tresca

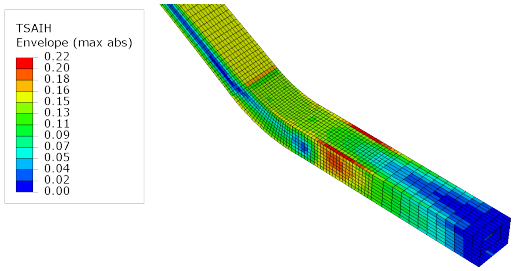

Figure 1.7: Tsai Hill

The analysis shows that the points with the highest stress are coinciding with the end of the deck while it remains roughly constant on the tapered section.

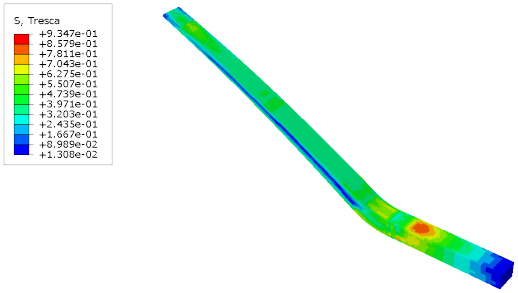

Figure 1.8: Tresca: core

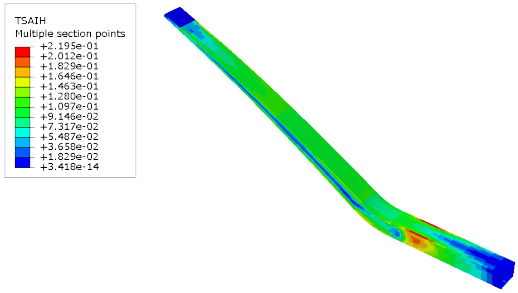

Figure 1.9: Tsai Hill: plies

1.2.2 Trampolines FEM analysis

As mentioned above, the new wings were produced with rigid trampolines to facilitate the skipper's ergonomics. To evaluate reliability and determine the necessary thickness for an adequate safety coefficient, Finite Element Method (FEM) analyses were conducted, modeling the trampolines as shells. The analysis particularly focused on the most critical scenario, which involved placing the skipper's entire weight at the center of the upper end of the trampoline.

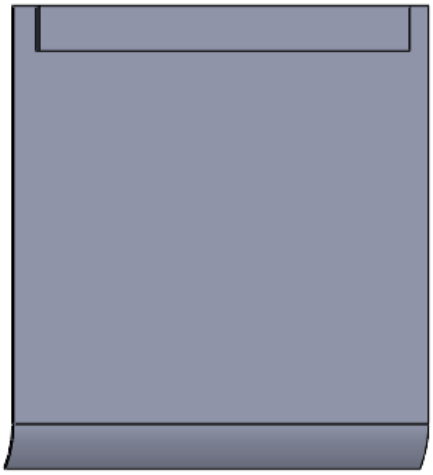

Figure 1.10: Trampoline

Following the initial analyses, longitudinal support was incorporated into the outermost section of the trampolines. This adjustment aimed to improve load absorption and distribution across the crossbars. The final design was constituted by a $5mm$ panel with an integrated $10mm$ reinforcement. This configuration is intended to achieve a good safety coefficient while minimizing overall weight.

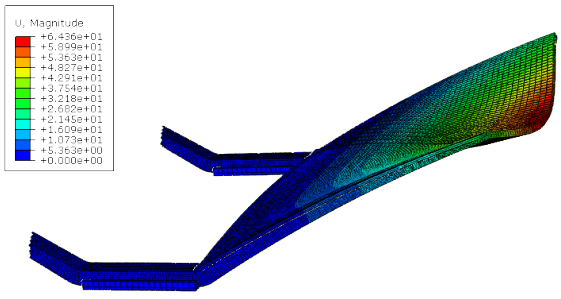

Figure 1.11: wing displacement

1.2.3 Comparison with previous wings

The new wings are just slightly heavier than last's year model, while being completely rigid and made out of basalt and recycled PET core. The new wings are thus more environmentally friendly both in choice of material and processes, as shown in the LCA analysis: previous year's wings contained pre-preg carbon fiber, that needed to be cured in an oven, while the new ones are vacuum infused and don't need any postcuring process.

1.3 Gantry

1.3.1 Overview

Upon the experience gained from the 2023 competition, it was decided to redesign the gantry with the goal of reducing drag with water, thus improving the takeoff performance of the boat. The new design needed to ensure the necessary mechanical strength to withstand the forces exerted on the component, without increasing the weight compared to the 2023 model. Another constraint was to design the gantry without modifying the current hull of the boat, utilizing the existing connection points on the transom. Additionally, specific aspects related mainly to the skipper's use have been addressed, such as modifying the rudder positioning and reducing splashing during the lifting phase.
Based on these goals and considering that the previous season's gantry remains usable, it was decided to develop two different design strategies that were not necessarily easy to produce and allowed for the use of less restrictive geometries, taking advantage of innovative technological solutions such as the use of 3D printing for the creation of the core.

1.3.2 Gantry Type 1

Initially, the idea was to cover the tubular structure of the gantry with a flat surface made of composite material that would be more hydrodynamically efficient and facilitate smoother contact between the component and the water. A CAD model was created to cover the tubular structure with a surface following its contour lines. Once the surface shape was obtained, it was decided to remove the internal tubular structure to reduce weight, thus creating a cover that was sufficiently mechanically resistant. The gantry cover also needed to accommodate the rudder housing and the hinges for connecting to the boat's transom. Additionally, a trapezoidal opening was made in the upper area of the gantry surface to reach the lower hinge connecting to the transom.

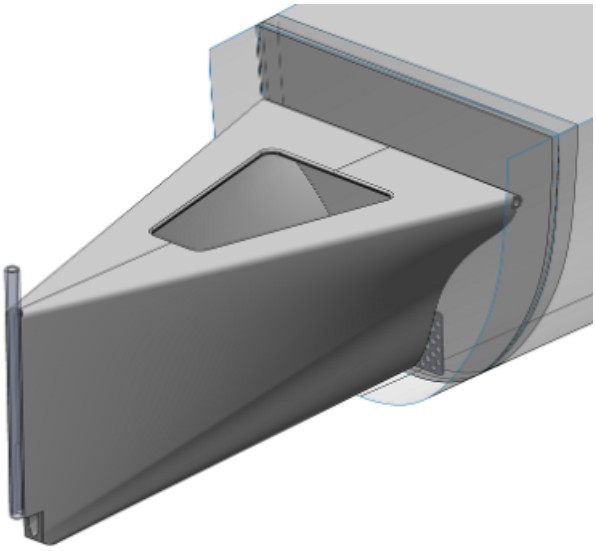

Figure 1.12: CAD of the Gantry Fairing

1.3.2.1 Engineering

Studying the component's behavior under stress allowed defining the best composite material sandwich that could provide the necessary strength while minimizing material usage. This was achieved through FEM analysis using Abaqus® software. Since the geometry of the gantry surface was complex to handle in the software, it was decided to represent the component as a single shell to which desired composite material layers, acting loads, and constraints were assigned.

1.3.2.2 Loads

The loads on the component are derived from CFD analysis of the forces exerted on the rudder, which are then transmitted to the boat's hull through the gantry. However, the loads are provided as concentrated forces at a point located on the rudder foil. To transfer them to the component, it was decided to simulate the rudder action using a wire coupled with a tubular component in contact with the gantry shell. The study considered only the highest loads recorded from the CFD analysis to be as conservative as possible.

	Fx	Fy	Fz
Load [N]	700	500	300

Table 1.2: Loading conditions of the rudder

1.3.2.3 Analysis Results

As evident from the applied loads, the most critical stress on the gantry fairing's performance is due to the torque resulting from Fx (caused by the length of the rudder).

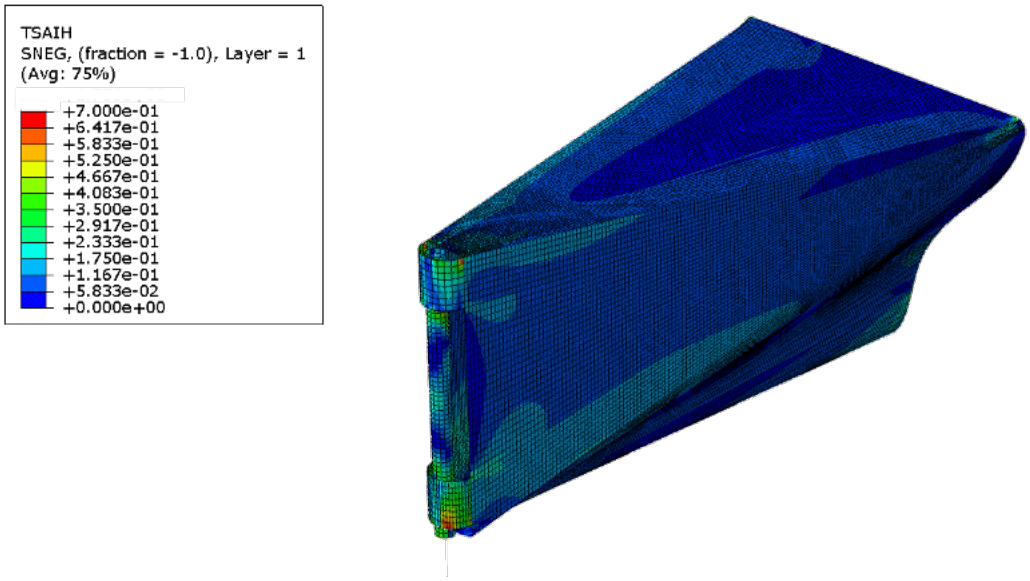

Figure 1.13: FEM of the Gantry

In order to ensure the necessary mechanical strength, it was decided to reinforce the most stressed areas with a greater number of skins and a thicker core, corresponding to the areas occupied by the tubes in the tubular gantry.

1.3.3 Gantry Type 2

To meet the requirements set for the gantry, a geometry was initially hypothesized to be as thin as possible. However, after finite element analyses, it was found to be inadequate for torsional stress. Therefore, a T-profile geometry was opted for.

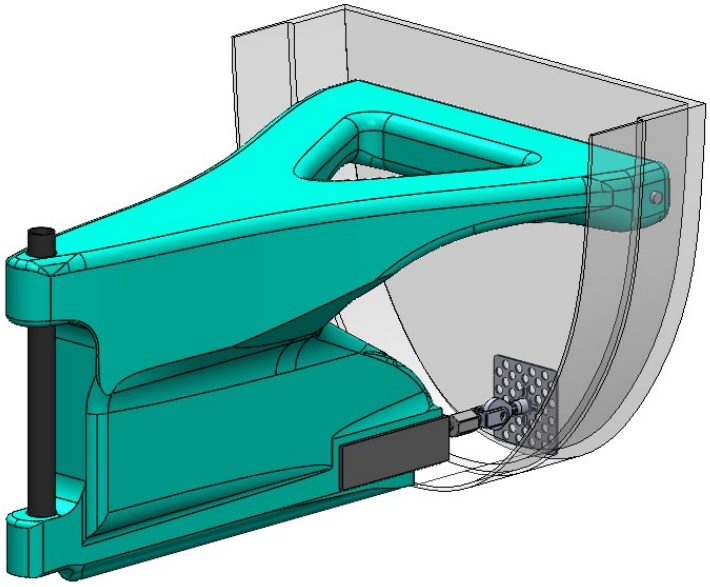

Figure 1.14: CAD of the Gantry

Regarding the materials used, carbon fiber was excluded in favor of a composite structure with a PET core and a basalt fiber. Once the effectiveness of the new shape was demonstrated, the focus shifted to topological analyses to reduce weight and dimensions. The gantry was designed to be compatible with the current joints, making it interchangeable with all versions. To achieve this, a basalt connecting fork had to be created. Lastly the rudder attachment was modified to raise the bar compared to the old gantry, aiming to achieve greater maneuverability after a confrontation with the skippers.

1.3.3.1 Analysis Results

Since basalt constituted the primary source of the overall weight of the gantry, these results enabled the identification of areas where the thickness of this material was excessive. Through a trial-and-error process and a series of FEM analyses, adjustments were made to vary the number of plies along the gantry's geometry

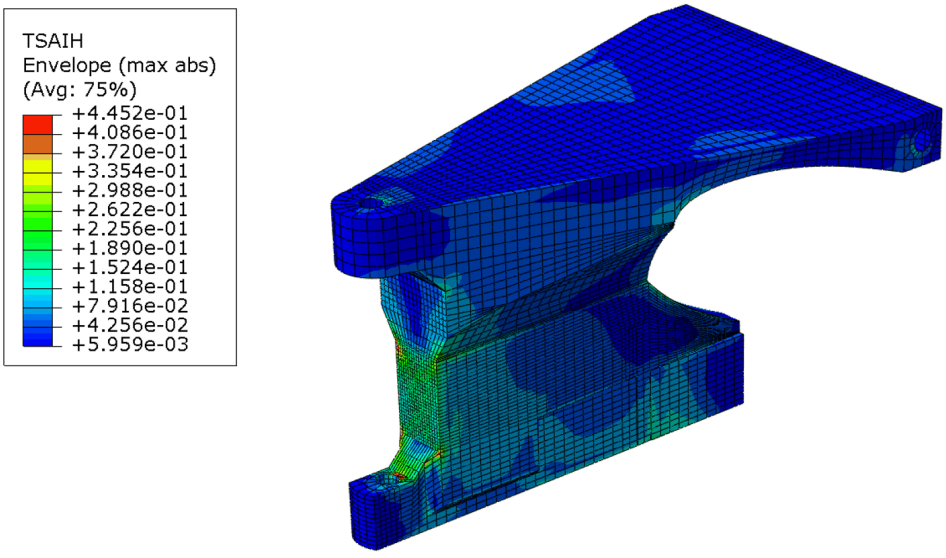

Figure 1.15: FEM of the Gantry

1.4 Rudder and main foil optimization

1.4.1 Input Data

The Matlab[17] code developed to optimise the planform shape of the foil utilises a series of variables enabling the analysis of performance across a wide range of possible foil geometries. At each iteration, the variables are subjected to dynamic minimum and maximum bounds, which adapt according to the values assigned to the respective parameters. Specifically, the input parameters used are:

- Span: This variable determines the wingspan length (Fig. 1.16).
- Leading Edge Points: Considering a plan view of the wing, five points are established between the centerline and the wingtip. These points are subsequently interpolated using a Bezier curve, resulting in the leading edge shape (Fig. 1.16).
- Chord Line: Length of the profile chord along the wingspan (Fig. 1.17). This value decreases non-linearly from the centerline to the wingtip. Once the leading edge points and the chord length along the entire wingspan are determined, the trailing edge shape is derived accordingly.
- Camber Line: For each wing section, it is possible to vary the profile shape by specifying a certain camber line length (Fig. 1.17). This parameter has a minimum value equal to the chord length for the corresponding section (symmetrical profile).
- Profile Points: An airfoil profile is constructed based on accumulated experience from previous years, considering the foil's usage conditions (Fig. 1.17). This profile is adapted along the wingspan, taking into account the chord line and camber line for each wing section.
- YawAngle and RollAngle: The wing geometry obtained with the previous variables is rotated about the yaw axis and the roll axis (Fig. 1.18).
- RollCurvature: The foils are not only rotated but also curved along the roll axis to explore even more complex geometries (Fig. 1.19).
- PitchAngle: This variable varies the pitch inclination relative to the wing profile's pitch axis. By doing so, it is possible to progressively reduce the angle of attack from the centerline to the tip, thereby achieving superior performance.

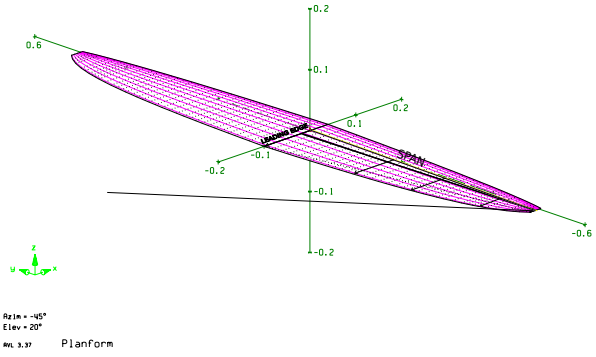

Figure 1.16: Span and LeadingEdge

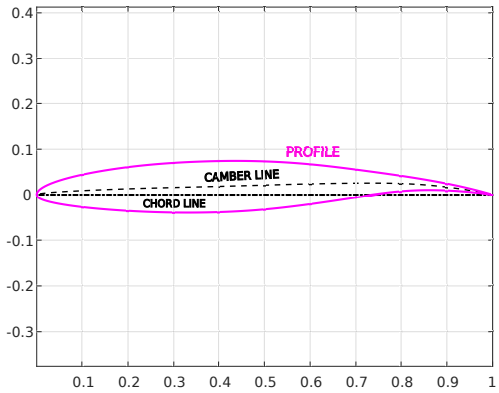

Figure 1.17: Profile

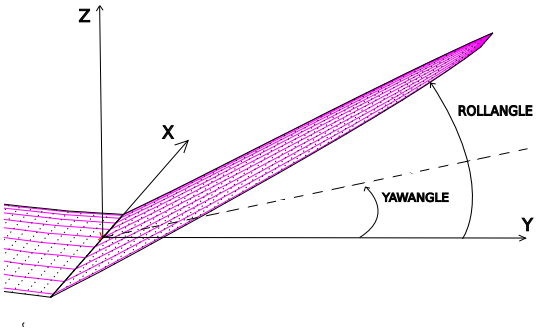

Figure 1.18: YawAngle and RollAngle

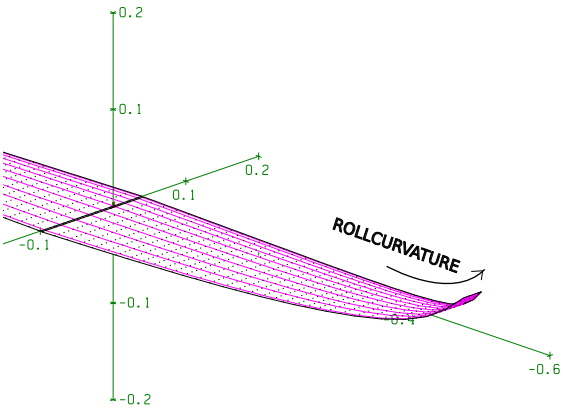

Figure 1.19: RollCurvature

Once the wing geometry is obtained, a desired lift coefficient (CL) is specified, and subsequently, the angle of attack (α) and the drag coefficient (CD) are calculated accordingly.

1.4.2 Objective Function

The Objective Function aims to minimise the drag calculated on the hydrofoil. In order to achieve this we first need a valid geometry to execute our calculation on. A series of controls are made to ensure geometry feasibility and the solution stay inside the problem's boundary. Next, an .avl type file is created with the geometry of the hydrofoil. As a result, aerodynamics calculations can be done with AVL (Sec. A.1.2.2). We assign the fitness to the drag of the foil. Further analysis is done to ensure that the pitching moment lays between a predetermined range.

1.4.3 Genetic Algorithm:

The implemented optimization algorithm is a Particle Swarm Optimization (PSO), which offers a good trade between convergence time and space solution exploration. The algorithm tries to mimic the behaviour of a swarm. The movement of each particle is determined by two main factors: its current velocity and its position in the search space. The velocity of a particle guides its movement towards promising regions in the search space. This velocity is adjusted iteratively relatively on the particle's own best position (local information) and the best position found by any particle in the swarm (global information). By continuously updating their positions and velocities based on local and global information, particles gradually converge towards the optimal solution. This process is driven by the principle of collective intelligence, where the swarm as a whole benefits from the experiences of individual particles.

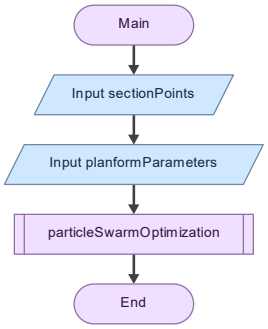

Figure 1.20: Main

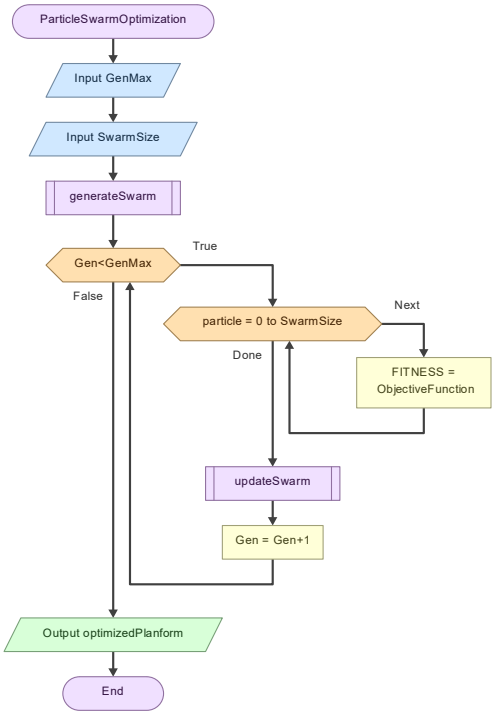

Figure 1.21: Particle swarm optimization

1.4.4 Final results:

Due to all the changes above mentioned, the code was essentially revolutionized. This provided a substantial improvement both in code performance, with convergence time reduced by over 40%, and in the geometries obtained, as the new foil's profile, while keeping the CL constant, has the CD 5% lower than last year's. The most promising geometries obtained have then been tested with CFD analysis.

1.5 Main foil vertical adjoint-based shape optimization

1.5.1 Overview

The following section is focused on the optimization of the shape of the main foil's vertical profile, in order to minimize hydrodynamic drag during the flight phase. Employing an adjoint-based optimization methodology, this task aimed to refine the geometry of the two-dimensional profile efficiently and accurately. The adjoint-based approach stands out for its precision in computing the sensitivity of the objective function, in this case the hydrodynamic drag, with respect to design variables, which in this application correspond to the vertical's profile shape. This method, which solves a set of primal equations (i.e. Navier-Stokes equations) and then a second set of adjoint equations, allows to understand how marginal changes in geometry can influence the desired objective, enabling efficient navigation in the design space. To implement this strategy, DAFoam® was used, an advanced open source software that integrates the adjoint approach within the OpenFOAM®[13] framework. This combination gave the necessary tools to conduct high-fidelity optimizations with a relatively low computational cost.

1.5.2 Adjoint-based optimization method

The adjoint-based optimization method is an advanced technique tailored for applications like minimizing fluid dynamics drag. It fundamentally relies on solving two interconnected sets of equations: the Navier-Stokes equations (primal problem), that describe the fluid flow behaviour, and the adjoint equations (secondary problem), specifically formulated to efficiently compute the gradients of the objective function(i.e. the hydrodynamic drag in our case).
This method's efficiency lies in its ability to compute gradients concerning a wide array of design parameters without increasing the computational demand. Although these adjoint equations are intricately linked to the primal set, their main focus is on capture how changes in design variables influence the objective function, offering a detailed view of the profile's hydrodynamic response to shape alterations.
Additionally, the adjoint-based optimization method not only facilitates a deeper understanding of how design alterations affect hydrodynamic performance but does so with remarkable computational efficiency. This aspect is crucial, as it enables focused and effective design enhancements without the extensive computational resources typically associated with high-fidelity simulations. Standing as a pivotal tool in aerodynamic optimization, this method offers a structured approach to improving performance metrics, guided by informed design modifications. Its computational economy, combined with the depth of insight it provides, makes the adjoint-based method a preferred choice for tackling complex optimization challenges in aerodynamics.

1.5.3 Case setup

In this section, the setup parameters for the hydrodynamic optimization of the main foil's vertical profile are outlied. As starting point, a two-dimensional O-type mesh has been constructed around the original profile, consisting of approximately 25000 cells (Fig. 1.22). Additionally, to effectively capture boundary layer effects, a mesh refinement is applied near the airfoil surface. Moreover, the progression of cells in the direction perpendicular to the airfoil profile is set to maintain a y^+ value lower than 1. The y^+ value represents the dimensionless distance from the wall to the first cell centroid, normalized by the viscous sublayer thickness, and it is defined as:

$$y^+ = \frac{u_\tau \cdot y}{\nu} \tag{1.1}$$

Where:

- u_τ is the friction velocity,
- y is the distance from the wall,
- ν is the kinematic viscosity of the water.

It is crucial to keep the y^+ value below 1 to ensure accurate resolution of the near-wall flow physics in computational fluid dynamics simulations, where maintaining proper boundary layer resolution is essential for an accurate hydrodynamic drag prediction. The angle of attack of the profile is set to zero degree, in order to simulate the straight-ahead sailing condition.

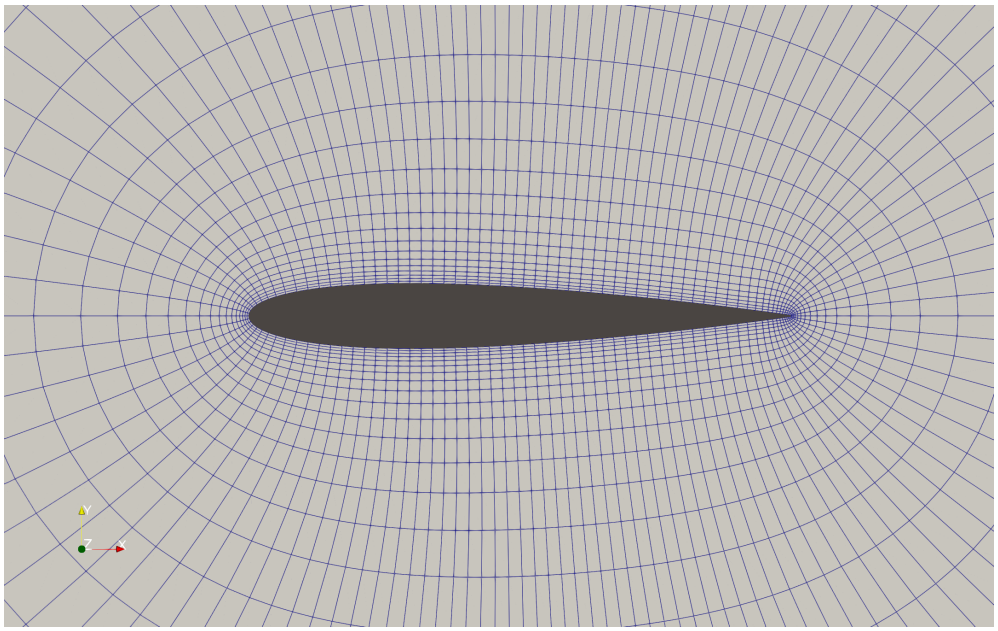

Figure 1.22: O-grid mesh of the initial geometry.

The fluid dynamics model employed is governed by the Reynolds-Averaged Navier-Stokes (RANS) equations. This approach averages the effects of velocity fluctuations, providing a computationally efficient yet sufficiently accurate representation of the flow around the main foil's vertical. The RANS model is particularly suited to this case as it strikes a balance between the need for high-fidelity predictions of hydrodynamic forces and the computational constraints associated with geometry optimization.
To solve the primal problem, namely the Navier-Stokes equations, the following initial conditions are imposed in order to mimic the open sea flight conditions:

- Freestream velocity magnitude $\vec{u}_\infty = 10\, m/s$;
- Freestream density $\rho = 1000\, kg/m^3$;
- Freestream dynamic viscosity $\mu = 1.716 \times 10^{-5}\, Ns/m^2$;
- Freestream turbulence intensity 5%;

Additionally, the following boundary conditions are imposed:

- The airfoil surface is treated as a no-slip wall;
- At the domain boundaries, uniform inflow conditions are set to match the freestream velocity;
- At the downstream boundary, pressure outlet conditions are defined.

The *simpleFoam* solver from OpenFOAM®[13] is used for flow simulations. For the adjoint problem, in particular the optimization problem, some constraints are needed, otherwise in a drag-reduction optimization process the airfoil will collapse to a straight line. Moreover, these constraints have been aligned with the results of prior structural analyses. The aim of these analyses was to detect the characteristics that the structure must have to withstand the loads encountered during flight phases. In particular, the same chord length of $70mm$ and the same profile thickness of $10mm$ of the old configuration was kept. At this point, the optimization process iterates between solving the flow equations, computing the adjoint, and updating the design variables until convergence is reached based on the objective function and design constraints. This structured process ensures a systematic approach to optimizing the airfoil's geometry, focusing on reducing drag while adhering to specified design constraints. The integration of high-fidelity simulations with advanced optimization techniques facilitates precise adjustments to the airfoil profile, driving toward aerodynamic efficiency.

1.5.4 Results and future work

In conclusion, the optimization process led to a reduction in drag coefficient from an initial value of 0.001801 to a final value of 0.001749, marking a significant 3% improvement. This enhancement is particularly notable for a symmetric profile at a zero-degree angle of attack. The solution achieved convergence within 11 iterations, underscoring the efficiency of the optimization strategy (Fig. 1.26).

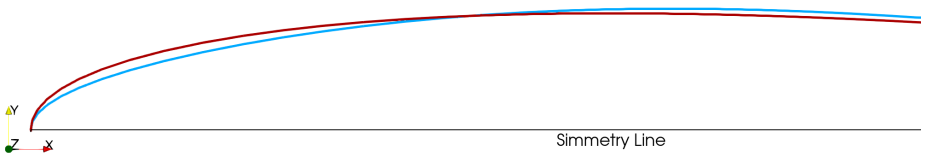

Figure 1.23: Detail on shape changes after adjoint optimization (Red initial geometry, Blue final geometry).

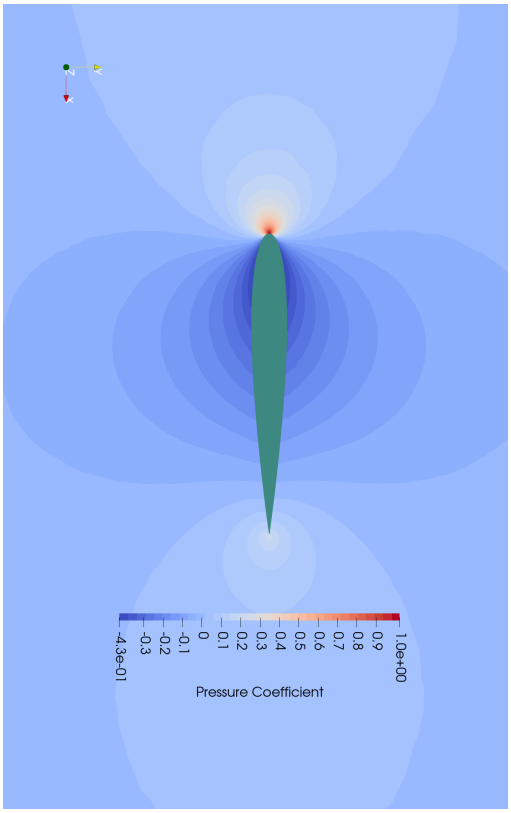

Figure 1.24: Pressure coefficient distribution pre-optimization.

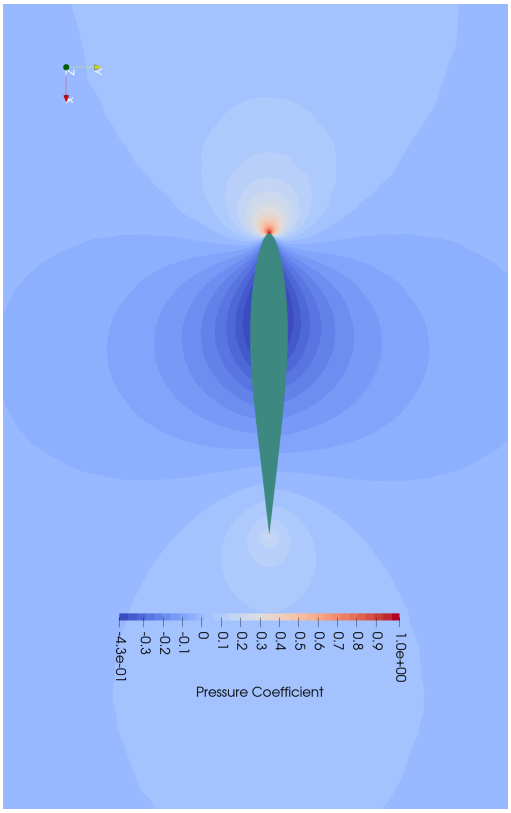

Figure 1.25: Pressure coefficient distribution post-optimization.

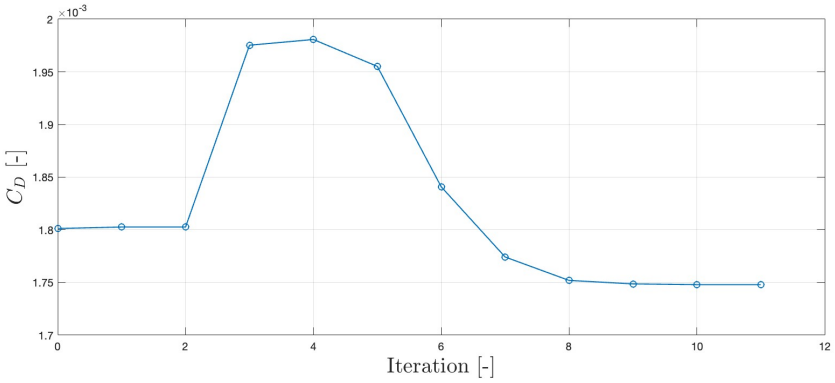

Figure 1.26: Objective-function convergence.

Opting to refine the 2D profile proved to be a prudent approach for minimizing drag during the flight phase, when vertical surfaces and foils are submerged. However, future work could explore the optimization the vertical section at the vetical-bulb intersection. Currently, the vertical and foil are optimized independently. Developing a model that simultaneously accounts for both the foil and vertical elements presents a challenging yet potentially rewarding opportunity to further elevate Febe's remarkable performance.

1.6 Foils performance under ventilation condition

1.6.1 Problem statement

A CFD study was carried out to investigate the hydrodynamic events that could occur when the foils are employed near the interface between air and water. Specifically, the aim was to achieve ventilation on the main foil during a regime of rolled flight, and assess the performance losses that this event could trigger. Hydrofoil ventilation refers to the phenomenon in which air gets drawn into the low-pressure region on the surface of a hydrofoil, disrupting the smooth flow of water over it. This can cause a significant loss of lift and an increase in drag, negatively impacting the hydrofoil's performance. This type of study was required to guide future developments of Febe Moth's height detection system, while growing the team's knowledge of potential problems associated with this new technology. Mostly, it aimed to set up a functioning model in anticipation of next year's foils redesign and point out the performance of the new rudder bulb under main foil ventilation conditions.

1.6.2 Methodology

To begin with, an extensive review of the available literature was conducted to understand the physical characteristics of the ventilation phenomenon and to clarify the reasons that could trigger such an event. From this analysis it was concluded, as expected, that ventilation takes place because of the presence of a strong low-pressure area on the suction side of the hydrofoil, generated through either high speed or high angles of attack. After reaching specific conditions, the pressure gradient between the water-air interface and the foil becomes so significant that air is drawn under the interface, generating a significant loss in lift and a spike in drag. But this is not the only mechanism inducing this phenomenon. Another important factor in this physical event is the boundary layer. In regions where the boundary layer separates from the hydrofoil surface, large vortices can form, creating zones of very low pressure that can suck air into the flow, initiating ventilation. Also, the high transport and mixing capabilities characteristic of the boundary layer, could enhance the tendency for air to be entrained into the water flow, around the hydrofoil near the free surface. Finally, simulations considering both the main foil and the rudder were set up. This choice resulted in a very high computational demanding meshing process. The domain was discretized using particular care in the near foil region, and refining the interface area placed at roughly one chord from the main foil. To carry out the simulations a RANS model was considered, joined with a VOF (Volume Of Fluid) approach to track and locate the free surface. The solutions were computed trough the use

of the interFoam®solver. Moreover, a k-omega SST turbulence model was selected to account for the turbulence effects that could impact in the production of ventilation. The model, comprehensive of all these characteristics, was already validated from a previous study presented in the Sumoth Challenge 2023 report.

1.6.3 Results

After achieving ventilation, it could be observed that the lift produced by the main foil drastically dropped by $36.4\%$and the drag generated rose by approximately 72% with respect to the initial values, highlighting the crushing impact on the foil's performances. These results are consistent with the ones found in the papers analyzed during the literature review.

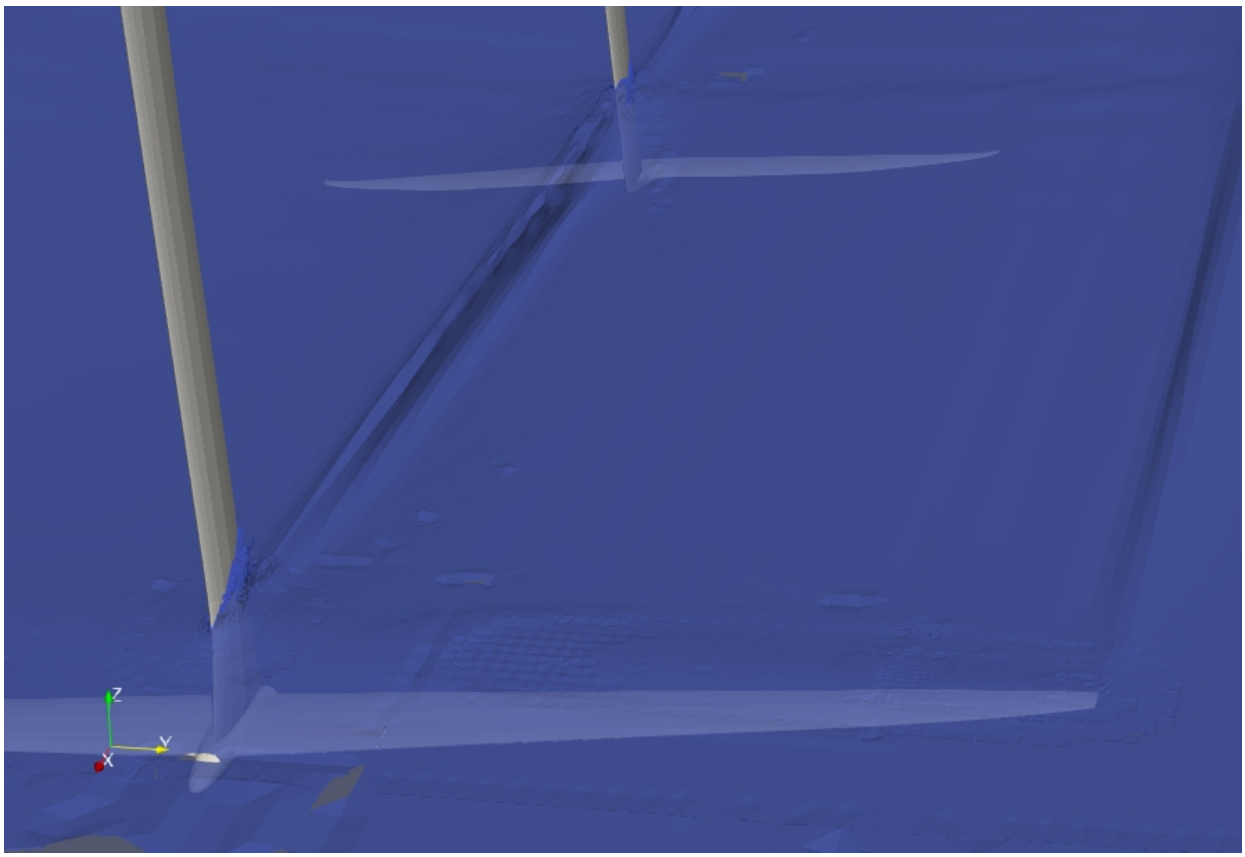

Figure 1.27: Air-water interface visualization.

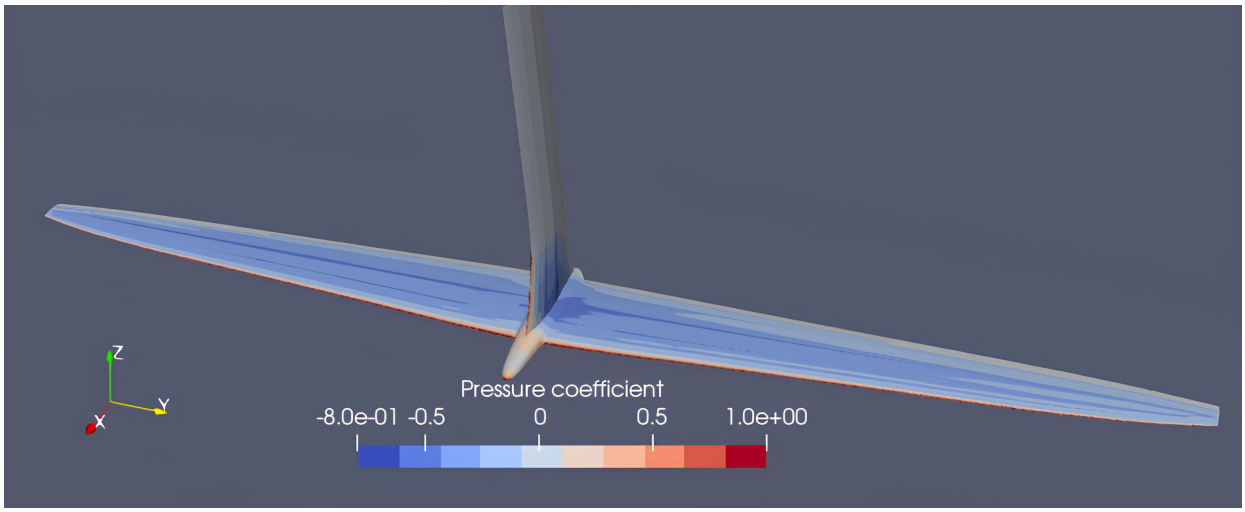

Figure 1.28: Pressure coefficient distribution on main foil at the beginning of ventilation.

1.7 Rudder bulb re-design for enhanced load durability

1.7.1 Overview

During the 2023 Foiling Week in Lake Garda, the rudder designed for the 2023 Sumoth suffered a failure that led to the detachment of both foil semi-wings. After an in-depth analysis of the recovered rudder parts (Fig. 1.29), it was found that the failure was due to inadequate load-bearing capacity of the bulb under the torque loads generated by the semi-wings during the vessel's flight phases. This section describes the redesign process aimed to enhancing the structural characteristics of the rudder bulb.
The goal was to improve the bulb's resistance to the torque generated by the lift while minimizing the impact of this process on the hydrodynamic performance of the rudder. The redesign focused on geometric modifications and structural reinforcement to achieve a balanced improvement in both durability and efficiency, ensuring the moth's competitive edge in high-stress sailing conditions.

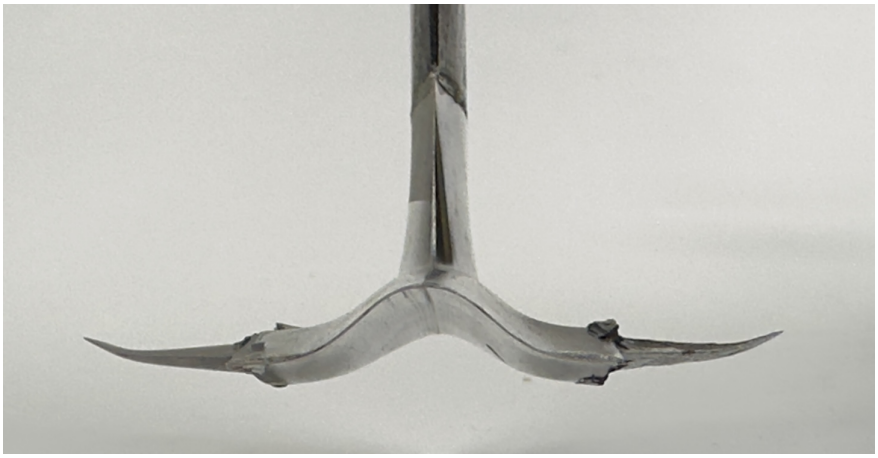

Figure 1.29: Broken rudder bulb.

1.7.2 New design requisites

To evaluate the suitability of the current rudder-bulb configuration to endure loads, when compared to the previous season's bulb, an Abaqus [16]®model was developed. As a result, it was opted to retain the current configuration while improving the bulb's resistance to loads through a new assembly technique. Specifically, multiple layers of unidirectional carbon skins

were applied around the semi-wings, in the direction of the wing span. This improved the bulb's capacity to withstand hydrodynamic torque produced by the foil's semi-wings. Additionally, modifications to the bulb's geometry were required to accommodate the necessary space for positioning the skins, the foil was also re-positioned rearward. In order to ensure optimal adhesion of the skins, modifications to the concave area of the previous bulb's pressure side were required: this comprehensive strategy aims to ensure the bulb's structural integrity under loads while preserving the rudder's hydrodynamic efficiency, without significantly altering the well-optimized geometry of the previous bulb design.

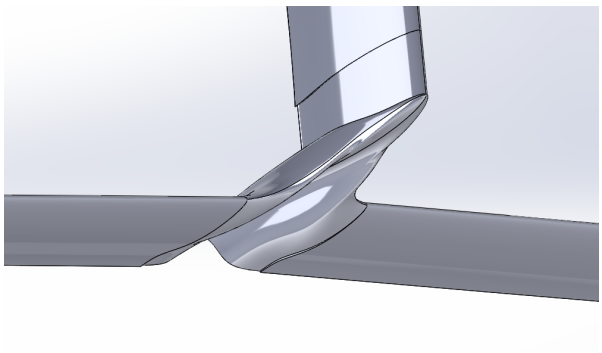

Figure 1.30: Old rudder bulb design.

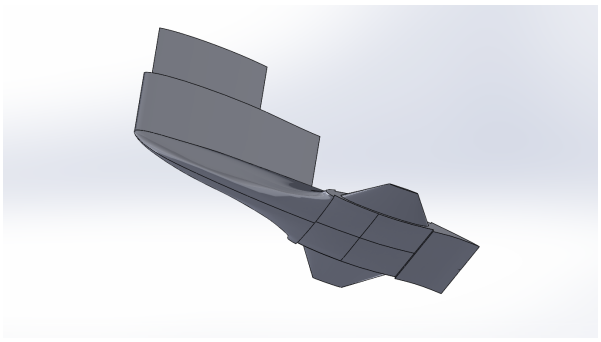

Figure 1.31: New rudder bulb design.

1.7.3 Design process

The already existing geometry, which was a result of an extensive optimization process, was used as a starting point to develop the new bulb geometry that meets the requirements mentioned above. Five different versions of the new bulb were created, featuring back-positioned semi-wings and a flatter pressure side. Subsequently, to identify the most efficient geometry (defined as the one with the best lift-to-drag ratio) a series of CFD simulations were conducted. Featuring identical initial and boundary conditions, chosen to simulate the conditions of flight in open sea:

- Freestream velocity magnitude $\vec{u}_\infty = 10\,m/s$;
- Freestream density $\rho = 1000 kg/m^3$;
- Freestream dynamic viscosity $\mu = 1.716 \times 10^{-5} Ns/m^2$;
- Freestream turbolence intensity 5%;
- No-slip condition on bulb surface.

After identifying the most effective geometry from the five variants, the chosen design was subjected to further refinement through adjoint optimization. This process aimed to reduce both viscous and pressure drag, all the while preserving the predetermined lift coefficient. This optimization was executed using the DAFoam software, ensuring that the final design not only adhered to the structural and hydrodynamic efficiency requirements but also aligned with the competitive demands of dynamic sailing environments. The freestream condition for the adjoint process are the same used for the previous CFD analysis. Additionally, to prevent the formation of wave-like shapes, a curvature constrain has been implemented on the bulb surface. The overall curvature, approximated as the maximum curvature, in the optimized design is restricted to not exceed 1.2 times the curvature found in the baseline design.

1.7.4 Results

The innovations applied to the rudder's bulb on Febe, followed an exhaustive design process and exploited innovative constructions techniques. Resulting in a significantly enhanced reliability without affecting its overall performance. This purposeful design, through an in depth optimization process and an efficient use of alternative materials, ensures a perfect blend of durability and hydro efficiency. Moreover, a positive side effect of the implemented solutions

was the possibility of reusing the existing aluminium mould for the rudder's foils, leading to substantial economic and environmental savings.

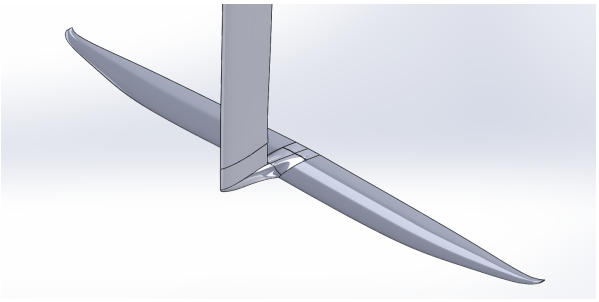

Figure 1.32: New rudder assembly.

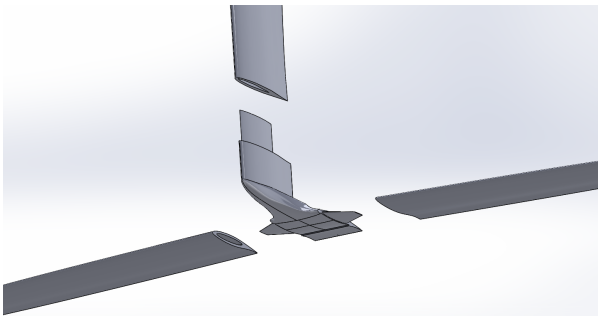

Figure 1.33: New rudder exploded.

1.8 Plies shape generation using Laminate Tools ®

The flat projection of the sequence of plies that makes up the foils was made using Laminate Tools®[15]. Starting from the CAD model of the mould, which consists of two halves that are closed together, the plies begin to be overlapped creating a layup starting from the internal surface up to the midline of the mould at the point of maximum thickness. Since the foil has a profile that becomes thinner towards the ends, the further away from the point of maximum thickness, the lesser the number of plies that make the layup at the desired point. To achieve this result, a flat surface that closes one half of the mould, a sort of "lid", was created in CAD, corresponding to the midline of the airfoil profile. When the plies of the layup cross the surface that closes the mould they are cut, gradually obtaining smaller plies that converge towards the center of the mould. In this way, the outermost ply will be the largest and within the foil, the plies will progressively become smaller. Once the geometry of the individual plies is defined, Laminate Tools[15] generates the flat projection of them which is used by the laser plotter for cutting.

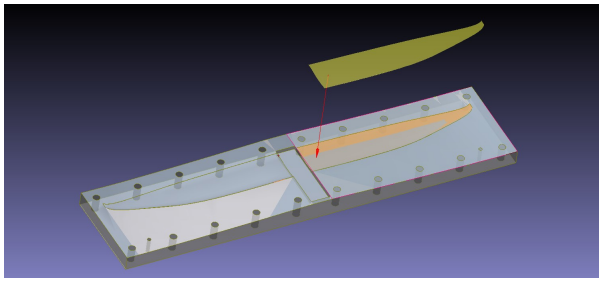

Figure 1.34: Ply from horizontal rudder.

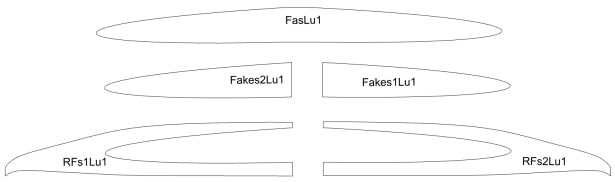

Figure 1.35: External carbon skin around the bulb.

1.9 Mechatronic system

This year work is centered around creating a more stable, robust, and scalable system to accommodate for a more complex electronic architecture. Overall the workflow is divided into three subcategories: the creation of a telecommunication network for managing the sensors, the introduction of a central onboard computer and the management of its peripherals, the development of a control algorithm to optimize the boat performance with the aid of simulation tools.

1.9.1 Configuration

For the next iteration of electronic system the plan is to use a wide variety of sensors on board: this is useful for the control algorithm since a larger data sample will describe with greater accuracy the dynamics of the boat, but also for training purposes of both the simulation tool and

the skipper by providing post-training data analysis in order to improve the performance. The sensors that are planned to be implemented are: a potentiometer to read the wand angle (for a boat with a "classical" configuration with wand), an ultrasonic sensor (for measuring the boat height with respect to water level substituting the mechanical wand), multiple IMUs (Inertial Measurement Unit), a GPS, a wind sensor and an encoder (to measure the boom position). Given the large amount of sensors, the development of a proper network to manage the large amount of information is needed. Furthermore, it would be widely impractical and not robust to singularly connect each module to its power supply and central computer. So the introduction of the CAN-BUS. The CAN-BUS is a standard for field bus, used in industry and automotive, that allows the exchange of messages between multiple nodes. Because of its architecture it's also very reliable, very robust to the external environment, and finally, for large applications, lighter in terms of weight. NMEA2000 [2] is a standard protocol in nautical applications that has been created by the *National Marine Electronics Association* , the implementation however has all been done by the team.
The onboard computer is a Raspberry Pi 4, a small, highly capable computer that has been fitted with ROS[7]. ROS (short for Robotic Operating System) is an open-source library of programs specifically developed to manage and control mechanical systems. The features that it offers are a wide variety of tools that help in the management and communication of information. It's also very modular, hence allowing an easy introduction of new sensors in future upgrades of the system.
Finally, the control algorithms are an improved version of last year's with the use of a Kalman filter for sensor fusion (to combine collected data) and control purposes. The boat is actuated by a servomotor controlling the flap of the main foil. A project for a motorized rudder (to control the vertical dynamic of the boat only) has been developed.

1.9.2 Sensors

As said in the previous section, multiple sensors are being added to the boat:

- Potentiometer: this sensor is fitted to measure the angle of the wand as the boat is moving forward. To fit it on the front of the bowsprit a custom piece has been designed to allow for both electronic and mechanical (the way the flap is normally operated) control. This way it is possible to sail the boat in training and, at the same time, to tune the control algorithm without the risk of an unexpected behavior.
- Ultrasonic sensor: this is also fitted on the front of the bowsprit. Its assembly mutually excluded with the potentiometer: the ultrasonic sensor allows a precise measurement of height of the boat with clear advantages compared to a traditional setup. In order to be used a custom mounting rig has been designed.
- IMUs: the inertial measurement units are used to measure the attitude of the boat as well as to complement the height measurement system. In fact, using a combination of the data collected, a better understanding of the spatial position is acquired through the Kalman Filter. The use of these sensors is a key element in the operation of stability control. However, for a correct operation, they need to be paired with a GPS. Mounted on the boat there are three IMUs positioned in IP68 boxes.
- GPS: the GPS works in pair with IMUs. When calculating the attitude of the boat IMUs allow for fast measuring. However, over a period of time, the small errors that are picked at each sample time are accumulated, creating a "drift" in the positioning. The GPS, with its higher sampling time, cannot be used for control, but it's used to correct the drift error of the IMUs. The GPS is mounted in a IP68 box inside the hull of the boat.
- Wind sensor: used to measure the apparent wind, it is mounted on top of the front spreader for an undisturbed evaluation.
- Encoder: a magnetic sensor mounted in a slot between the mast and its mounting point, it is used to measure the angle of the boom with respect to the boat.

1.9.3 Actuators

- Servomotor: mounted on top of the main foil, connected with the Raspberry Pi 4, it is the connection between the electronic system and the mechanical system. The servomotor is connected to a rod that goes inside the main foil and fixed to the top of the flap, allowing movement.

1.9.4 Communication network

The Controller Area Network (CAN-Bus) is a communication network enabling multiple devices to exchange data with one another. It employs a multiplexing method where each device utilizes serial transmission. When a device intends to transmit data, it generates a sequence of bits, denoted by 0 for low voltage and 1 for high voltage. This sequence is then passed to a transceiver, which splits the signal into two lines: CAN-High (CANH) and CAN-Low (CANL).
During standby periods when no message is being transmitted, both CANH and CANL maintain the recessive bit value of 1, holding the same voltage. However, when a dominant bit (0) is transmitted, CANL voltage drops, while CANH rises. At the receiving end, the difference between these voltages is detected. This design ensures robustness as any electromagnetic interference affects both lines equally, maintaining the voltage difference and ensuring accurate data reception.
The CAN architecture has been divided into abstract layers:

- Physical layer: this defines the lowest layer of CAN protocol stack and serves to define the electrical characteristics of the system such as voltage, communication speed, pin assignment, end resistance.
- Data link layer: manages the transmission of data frame by the device to the network. It handles arbitration, when multiple devices want to transmit simultaneously, error detection and bit stuffing.
- Network layer: this handles some network specific information such as segmentation and addressing.
- Application layer: this defines the message composition and is specific to the application used.

Components:

- STMF103C8T6: the specific microcontroller has been chosen because it has already implemented some functionality of the physical layer as well as libraries.
- MCP2551 transceiver: used to convert the signal from single-ended to differential on the CANH and CANL lines.
- Terminal resistors: used between the CANL and CANH lines to avoid signal reflection.
- 5 poles cable: to connect the equipment, used to transmit the can messages.

The set of microcontroller, transceiver and sensor are often referred to as a node(Fig. 1.36).

1.9.4.1 CAN-bus operation

All systems transmitting on the bus use the same message configuration which is fixed. Because all nodes share the same bus, it can happen that two nodes are requesting to transmit simultaneously. In this case an arbitrage system called Carrier Sensing Multiple Access Collision Detection assigns the priority to the node with lower identifier. The message structure is:

- Start of Frame (SOF), single bit: marks the beginning of a CAN message and serves as a synchronization signal for the receiving nodes. It is always dominant (0), since the bus normally assumes the recessive bit (1) when idling and helps to establish the timing for message reception.

- Identifier (ID), 29 bit: a number representing the meaning of the message. Is transmitted from the most significant to the least. In particular NMEA uses the 29 bits identifier which is an extension from the basic 11 bits.
- Control Bits, 2 bit: the first bit is a flag that distinguishes between the standard ID (11 bits) or the extended (29 bits). The second is reserved for future expansion.
- Data length code (DLC), 4 bit: specifies the number of bytes transmitted in the message payload.
- Data field: this field has the actual information a node wants to transmit, the length is determined by the DLC.
- Cyclic redundancy check: is used to control that the message has been transmitted correctly, it contains a checksum calculated from the data
- Acknowledgment (ACK): indicates whether a message was received correctly or not.
- End of frame, 7 bit: marks the end of the message, it is always a sequence of 1.

Furthermore, in order to not confuse a string of 1 with the idling bus, every 5 consecutive recessive bits, an additional dominant bit is added. This practice is called bit stuffing. When interpreting the message the bit stuffing is removed returning to the original message to be read.
The arbitration method is equivalent to all other CAN application: when two or more nodes are communicating the priority is assigned to the node that transmits a dominant bit, while the other transmits a recessive one. The node that loses priority will re-attempt the transmission after the first message is finished.
The creation of the physical layer was done in accordance with NMEA standard: 5 poles cables (including shielding) were chosen. For the network architecture, a bit rate of 250kbit/s was used. The number of nodes used is significantly smaller than the network-defined maximum. The data link layer is partly managed by the software that we implemented with the microcontroller. The functioning was done according to ISO 11783-3 [11] standard, additional requirements specified by the NMEA standard may have been implemented.
All messages are read by a single node, composed like the others, that retransmits via serial communication the messages received to the main computer. A custom identifier is added to the message so that the main computer can assign the type of data received.
For the setup, the receiving CAN node and the Raspberry Pi 4 board have been inserted in a custom waterproof casing located inside the hull (hinged to the underdeck); similarly, the power source composed of a 5 cell lithium-ion battery is inside a nearly identical casing. For safety reasons, the connection to the system can be cut by a kill switch located on the deck.
Every node of the network was completely engineered and produced by our team. All the cases for the devices are custom-made and their waterproofness has been tested in our laboratory. All the circuit boards were designed, soldered, and tested by the team and the choices made for what concerns the components and the algorithms were aimed to minimize the power consumption of the system while maintaining the performances required to control effectively the dynamics of the boat.

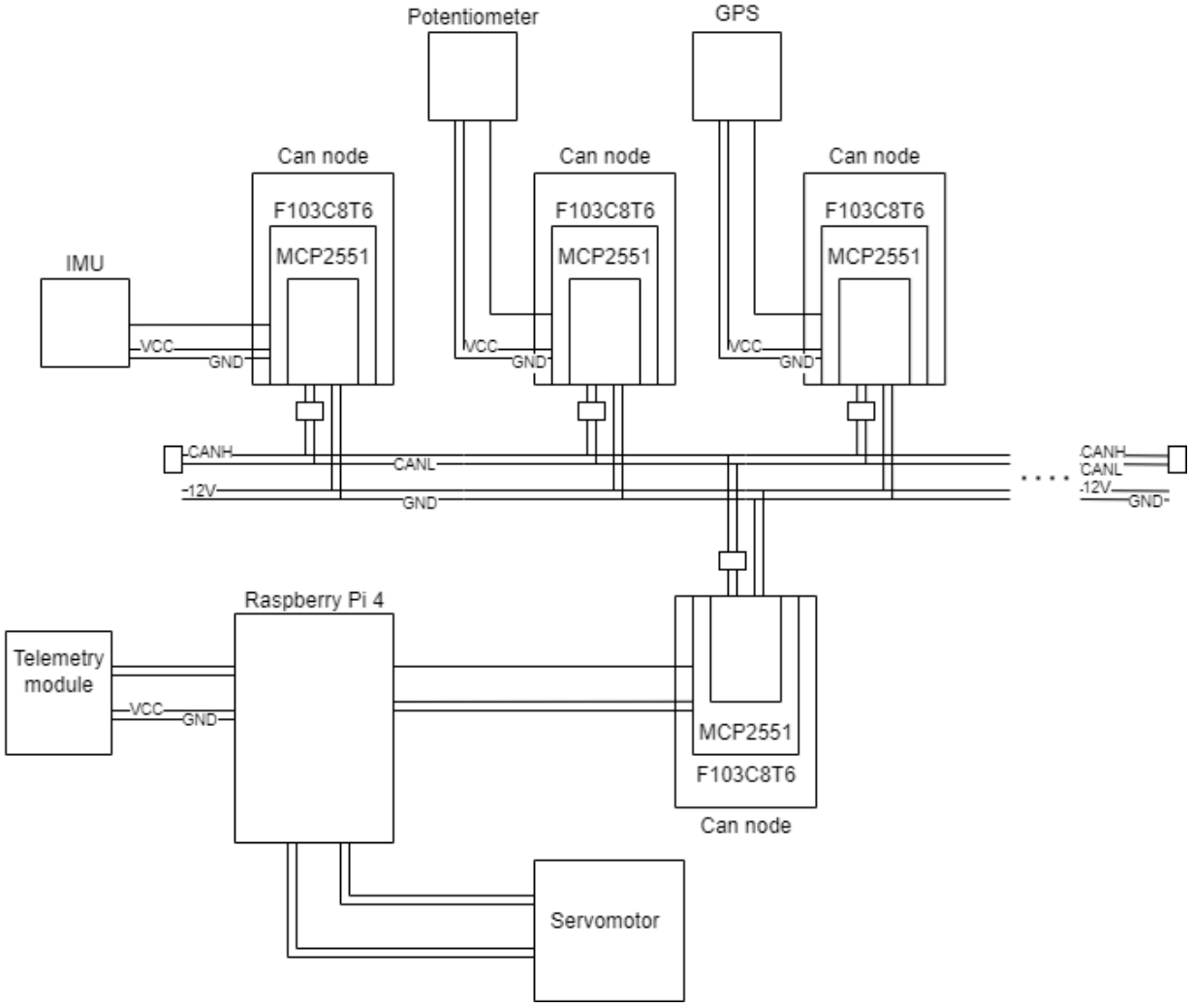

Figure 1.36: General scheme of onboard electrical connections

1.9.4.2 Final considerations on can-bus

The development of this system was instrumental for the growth in complexity that is expected for the successive generations of foiling boats. The application made the management of the electronics and specifically of the wiring much less intricate and less prone to faults. In fact, unless there is a power problem, the system will continue its execution even in the case of multiple sensors' failure.
During the implementation, it has been found that some of the NMEA requirements were limiting the potential of the bus. One clear example is the bit rate, which for NMEA systems needs to be $250kbit/s$. With the system we developed it is not difficult to maintain a bitrate 4 times higher: $1Mbit/s$. The lower bit rate does not compromise the overall performance since it's enough to allow all sensors to have a more than reasonable frequency for sampling and sending the data. This limitation was created because the NMEA standard was thought to work on large vessels.

1.9.5 Onboard computer and ROS

1.9.5.1 ROS architecture

At the heart of the setup lies the Raspberry Pi 4 single-board computer, equipped with the Ubuntu operating system. This arrangement gives developers great leeway while being at the same time easy to use and to replicate.
The SBC (short for single-board computer) is connected to the CAN bus through the F103C8T6,

which sends all the data it receives to the Raspberry Pi 4 using an SPI-based serial connection. Connecting to and managing the SBC from an external computer is achieved using the Secure Shell Protocol (ssh) over a local Network, while the telemetry communication is made possible by an antenna system connected via uart to the system.
The recording of all the data that arrives to the on-boat computer is made possible by a simple button, whose functioning is governed by a ROS node.
ROS, short for Robot Operating System [7], is an open-source framework designed to help with the development of robot software. Despite its name, ROS is not an operating system, but rather middleware that operates on top of a host operating system (in our case Ubuntu). It provides services such as hardware abstraction, device control, communication between processes, and package management. ROS offers a set of tools and libraries that aid the creation of complex robotic systems. These include drivers for various sensors and actuators, algorithms for localization and mapping, simulation environments, and more. One of the key features of ROS is its modular architecture, which allows developers to design systems using a distributed network of simple programs performing simple tasks (nodes) communicating with each other via standard messages (topics).
ROS's modular architecture enables to break down complex systems into smaller, more manageable nodes, facilitating the design process, testing, and maintenance. This approach facilitates the management of systems that involve various subsystems like data processing, sensor fusion, and control algorithms. Integration with other simulation environments allows testing control algorithms in a virtual environment before deployment.

1.9.5.2 Data acquisition and recording

Data from the sensors are communicated to the computer using the microcontroller stated previously sending data that arrive real-time through the serial port. All data coming from the sensors need to be pre-processed. Have it be the analog reading from a potentiometer returning a digital value in a certain range to be translated into an angle or adding the level of uncertainty to the data so that future algorithms can weight its data accordingly. All sensor data also need to be published in a given format supported by ROS so that it can be used and seen correctly by all packages.

As a whole, the ROS framework manages and exchanges a substantial volume of information ($messages$) with several external interfaces, continuously sending and receiving data. In such a complex architecture, properly saving the data is essential to conduct further analysis and validations. To address this need, one of the most valuable tools provided by ROS is the "$rosbag$". This feature enables the recording of the data into a $.bag$ file as it is received, ensuring the information integrity and preventing data losses.
A bag file can store data from either a single $topic$ or all active topics simultaneously. Moreover, different message types (e.g. floats, strings, etc.) are automatically classified and recorded with their respective timestamps based on the sending frequency, preventing downsampling.
The sailboat architecture includes:

- Separate topics for each sensor (Encoder, Potentiometer, Windex, IMU, GPS), derived from the CAN-reader node;
- A topic with the boat's height estimation (from z_{est} node);
- A topic with the reference trajectory, serving as input for the controller;
- the $FlapAngle$ topic, containing the controller's output;
- the $ServoAngle$ topic, providing the input signal for actuating the servomotor;

Recording playback: Once recorded, a bag can be conveniently handled as a file and replayed on a computer without the necessity for specific electronic devices.
This enables access to a readily available dataset for offline analysis, significantly improving the efficiency of troubleshooting and fine-tuning of the sailboat control.
Furthermore, by playing back a bag, it is possible to reproduce the boat's configuration and dynamics which can be visualized using dedicated tools or simulation environments.

1.9.5.3 System state estimation

- **Height:**
  From the potentiometer's reading and the knowledge of the geometry of boat we can derive the relationship between the angle of the wand and the height of the boat to the water. This faithfully reproduces the current physical system and is used both to have a simple and correct reading of the height of the boat but also to study the differences between our solutions and the old way of controlling the boat.
  This estimation can be further enhanced by adding the knowledge of pitch of the boat from the IMU's readings and through sensor fusion techniques with the accelerations also from the IMU's, and other sensors returning the distance from the boat to water such as Ultra-sonic sensors.
- **Yaw, Pitch and Roll:**
  One very useful information is the orientation of the boat in space.
  This is retrieved from the IMU and can be improved by fusing the data coming from multiple IMU's
- **Position in space:**
  Other than the height, to reconstruct the path followed by the boat we need to know it's planar position in space.
  This can be done through the GPS's latitude and longitude readings and improved through sensor fusion with the acceleration readings coming from the IMUs.
  The algorithm used for this estimation comes from the $robotlocalization$ package from the ROS Community.
- **Velocity's magnitude and direction:**
  From the same sensors as before we can retrieve the speed of the boat through space, which is the main data to understand the performance of our work.

1.9.6 Control

1.9.6.1 PID main flap control

The PID controller (Proportional-Integral-Derivative) is used to dynamically adjust the amplitude of the flap angle in response to variations in the boat's height relative to the water surface. This control configuration has been chosen only for initial testing. The performance is superior than the mechanical configuration but the simplicity of it makes for a less sophisticated system, the controller planned to operate is discussed afterwards.:

Furthermore, it is important to remember that the flap angle is subject to saturation dictated by mechanical limits, which will therefore interfere with the integral action of the controller. Consequently, a PID controller with anti-wind-up effect has been implemented as depicted in the figure.

1.9.6.2 Servo control

The relationship between the flap angle and the angle of the servo, obtained experimentally, could be reasonably approximated with a first-order polynomial. The following linear function guarantees the best fit ($R^2 = 0.9894$):

$$servoAngle = -1.778 * flapAngle - 18.6878 \tag{1.2}$$

1.9.7 Telemetry

In order to provide real-time monitoring and some initial data collection capabilities, a telemetry system has been designed. By leveraging ROS2 modularity and LoRa communication technology, we were able to offer a robust and low power-consuming solution to transmit vital data from onboard sensors to a ground station.
LoRa, short for Long Range, is a wireless communication technology that operates within the

sub-gigahertz frequency bands, 433MHz in our case. It employs a modulation technique called chirp spread spectrum (CSS), which allows the transmission of data up to 8km at 980 bit/s.

1.9.7.1 Data collection

The data needed to be sent is asynchronously collected by a node within the ROS network. Every time a sensor outputs a new datum, the node encodes it and saves it in its data structure, marking it as fresh. Then, using a separate thread, two times every second, when all data is marked fresh, the node sends the packet to the outgoing buffer of the LoRa module.
Each packet sent by the module contains a data structure of 19 Bytes. Each variable is encoded using the minimum possible number of bits, considering the maximum possible value that each variable can assume. Just before sending the packet, a 16-bit error detection code is calculated and sent with the data.
Upon reception, a microcontroller at the ground station aligns and reconstructs the incoming data packets. It then verifies the integrity of the data using the attached error correction code. If the packet is deemed intact, the data is relayed to a computer, where a dedicated application visualizes the information. The visualization tool displays the sailboat's position on a map, utilizing the latitude and longitude coordinates. Additionally, the application generates appropriate graphs to represent other data metrics such as riding height, heading, speed, roll angle, and pitch angle. These visualizations aid the ground crew in monitoring the sailboat's performance and making informed decisions.

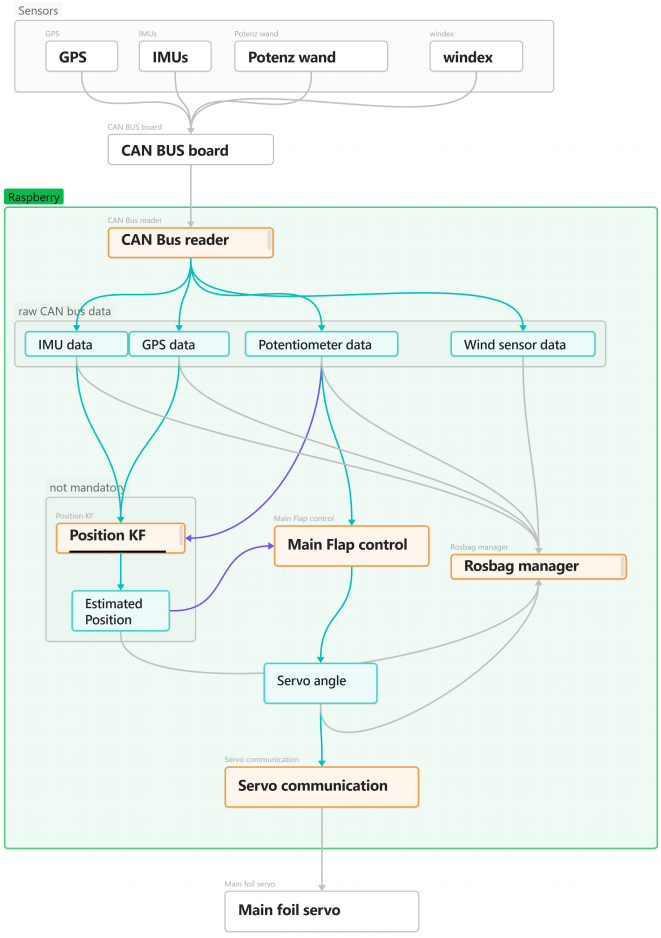

Figure 1.37: ROS architecture

1.9.8 Control algorithm and simulation tools

The control algorithm is based on last year developed structure. For initial testing a simple controller is designed that is explained previously. This serves to ensure that the fundamental aspect works correctly. However, afterwards, a Kalman filter will be implemented for state estimation and sensor fusion. The main difference in implementing it is the use of ROS, but the structure is analog to the other. The data sampled from different sensor is fed in the system and the output is the state of the boat such as position and velocity.

1.9.9 Study on rudder control

In addition to the keel flap control system, a rudder control system was designed. This system was intended to aid the skipper in finding an optimal configuration for flight control. The electronics would only operate as a pitch control measure substituting the handle that the skipper moves during takeoff and pace setting. In no way does it interfere with the yaw of the boat. The system was conceived to include a stepper motor inside the rudder tubular section acting on the screw that regulates the foil angle of attack. This system would benefit the skipper by reducing the response time, especially during takeoff.

- Electric stepper motor: used to rotate the screw inside the rudder. It has been chosen for its ease of use, because of PWM (pulse with modulation) control.
- Joystick: positioned at the tip of the tiller extension, it has two buttons for motion control. Inside a custom designed board is used to convert the helm inputs into physical signal for the motor.

2 MANUFACTURING AND COST ANALYSIS

2.1 Overview

The 2024 season saw the team engaged in a significant refit of last season's boat. Key updates included the redisign of rig, wings, gantry and deck. To track these changes, the team meticulously recorded resource usage, comparing actual consumption with estimates based on available documentation and historical data. To facilitate this process, a new accounting system based on the Odoo[14] platform was introduced, significantly easing the traceability of all team cash flows. The collected data were then organized and analyzed using Microsoft Excel[4].

	22-23 Season	23-24 Season	Variation	Budget left 23-24
TOTAL [**SuMoth$**]	9063.19	9838.59	+775.39	161.41

Table 2.1: General cost Overview

2.2 Main modifications

The modifications to the new prototype led to an increase in overall costs for several reasons. First, there was a need to strengthen the weaker elements of the previous design. Second, the rig components were updated, and interchangeable parts, including two gantries, were incorporated. Finally, the exploration of new production techniques, notably 3D printing for moulds, contributed to the cost increase.

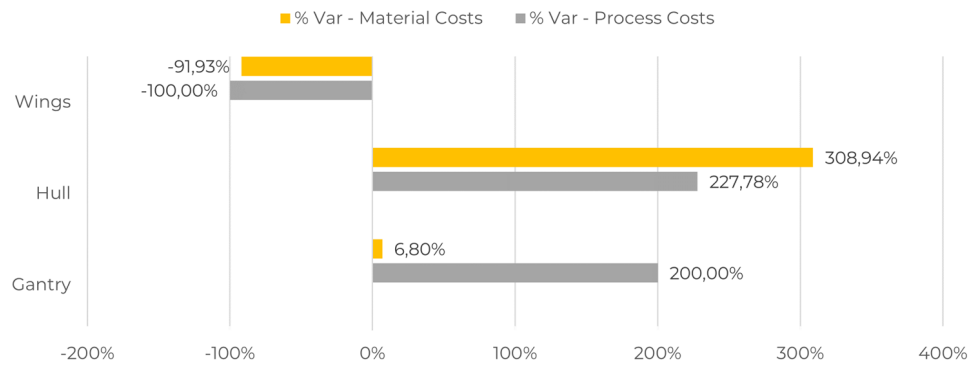

Figure 2.1: Percentage variation in Structural costs due to materials and processes

The deck was significantly reinforced, resulting in an increase in weight and cost.

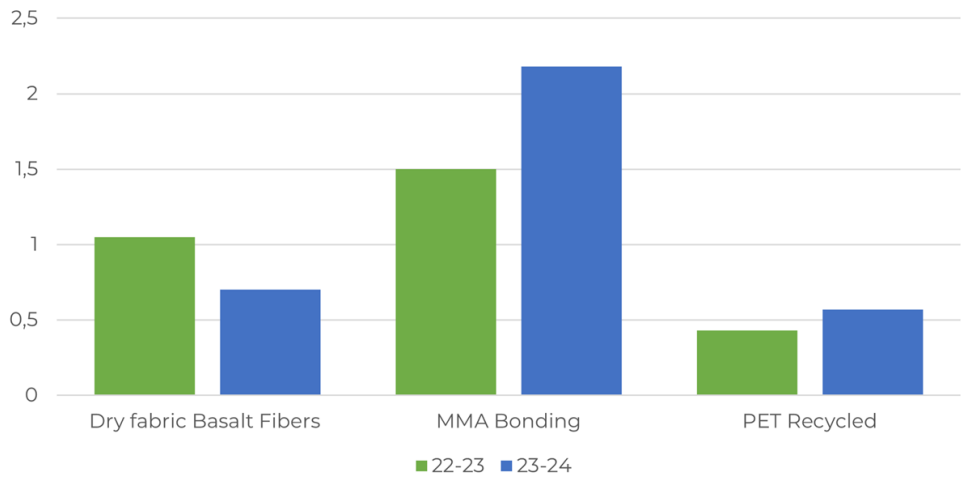

Figure 2.2: Deck materials [kg]

Comparing the current structures with those from the previous season, a substantial saving is evident, mainly attributed to the choice of materials. With experience gained using basalt fiber and thermoplastic resin, it was possible to expand their application, moving away from more polluting and expensive carbon and glass fibers in the construction of wings and gantries.

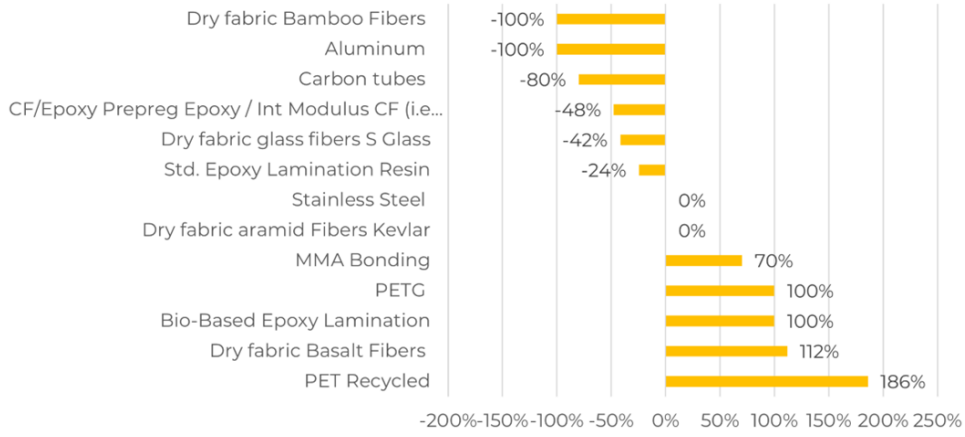

Figure 2.3: Percentage variation of total costs divided by material

To enhance synergy between the boat and the skipper, in addition to introducing a rigid design for the wings, the entire rigging system has been updated completely with more modern and high-performance components from Harken[9] and Gottifredi Maffioli[8]. Although these changes were costly, they will allow for significant improvements in the precision and fluidity of adjustments.

	TOTAL [SuMoth$]
22-23	2235.95
23-24	2585.72
Variation	**+349.76**

Table 2.2: Rig cost

Regarding the moulds, it was partly possible to eliminate the need for them. The wings design was simplified and optimized to allow production by bench infusion without a mould. The core of both new gantries was preformed to allow their creation by hand lay-up, also without the need for moulds.

	Weight [kg]	Total cost [SuMoth$]
Gantry Type 1	1.15	252.3
Gantry Type 2	3.27	14.4

Table 2.3: Weight and Total Cost of Gantry Types

However, the desire to experiment with 3D-printed moulds yielded interesting technical results but incurred high costs in SuMoth$ terms, mainly due to the size and characteristics of the material used for the fairing mould.
The outcome of all these considerations resulted in savings due to the use of more sustainable materials in structures, but also an increase in costs related to moulds. These variations clearly impacted the cost distribution , with experimentation with the new type of moulds becoming one of the most significant cost.

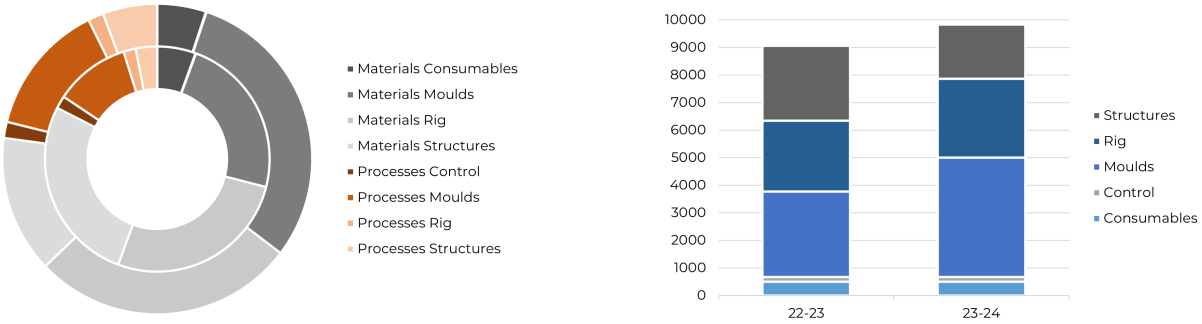

Figure 2.4: Costs distribution [SuM$] (Materials and Processes)

2.3 Upcycled and remanufactured parts

Parts of the rigging, along with the bowsprit and wand mechanism, will be fabricated by repairing and modifying components salvaged from the disposal of last year items. Other parts, such as the main foil and the rudder, will be remanufactured at ReFraschini [6] facility to match last season's specifications, using out-of-shelf-life fibers supplied by CIT [3]. The objective is to eliminate production defects identified in the old components through refining of the manufacturing techniques.

2.4 Main effects on weight

Analyzing only the structure that make up the boat, it is evident how the more sustainable choices made inevitably involved a compromise in terms of weight.

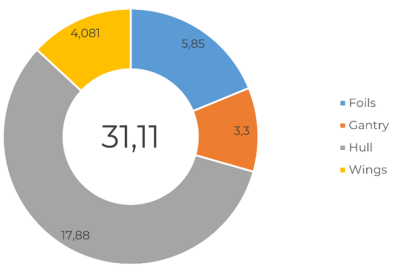

Figure 2.5: Total weight 22-23 [kg]

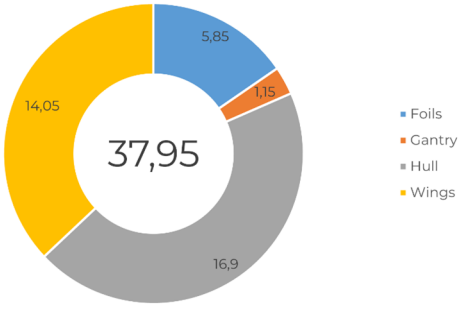

Figure 2.6: Total weight 23-24 [kg]
Only Gantry Type 1 was considered

2.5 Conclusion

In conclusion, the team made significant design choices and introduced numerous new solutions to reduce the cost of its boat. However, it also decided to invest the remaining of its budget in SuMoth$ to explore different designs for individual components and new production techniques with the aim of optimizing costs in the future.
The complete list of all materials that will be involved in the manufacturing process is provided below highlighted in blue (re-manufactured parts) and green (new parts).

Variations	Group	Subgroup	Part	Process	Machine time [h]	Material	Quantity	Unit	Condition	COSTxH [SuM$/H]	PROCESS COST [SuM$]	COSTxUoM [SuM$/UoM]	MATERIAL COST [SuM$]	TOTAL [SuM$]
	Consumables	Consumables	Infusion Material			Release agent Wax	1,00	Kg	New	0	0	50,0	50,0	50,0
	Consumables	Consumables	Infusion Material			Vacuum bagging Peel ply	40,00	Sqm	New	0	0	5,0	200,0	200,0
	Consumables	Consumables	Infusion Material			Vacuum bagging PVC vacuum hose	50,00	mt.	New	0	0	1,0	50,0	50,0
	Consumables	Consumables	Infusion Material			Vacuum bagging Spiral tube (inf.)	25,00	mt.	New	0	0	1,0	25,0	25,0
	Consumables	Consumables	Infusion Material			Vacuum bagging Tacky tape	2,00	15m roll	New	0	0	8,0	16,0	16,0
	Consumables	Consumables	Infusion Material			Vacuum bagging Vacuum bag	80,00	Sqm	New	0	0	2,0	160,0	160,0
	Control	Rudder assembly	Foil Control Mechanism	Machining (CNC)	3	Aluminum	0,40	Kg	New	40	120	10,0	4,0	124,0
	Control	Rudder assembly	Rudder Bar			Carbon tubes	0,50	Kg	Upcycled	0	0	0,0	0,0	0,0
	Control	Rudder assembly	Stick			Wood Others	0,30	Kg	New	0	0	0,0	0,0	0,0
	Control	Wand assembly	Bowsprit			Carbon tubes	0,40	Kg	Upcycled	0	0	0,0	0,0	0,0
New part	Control	Wand assembly	Wand			Aluminum	0,30	Kg	New	0	0	10,0	3,0	3,0
New part	Control	Wand assembly	Wand	Laser (CNC)	0,25	Carbon rods	0,25	Kg	Upcycled	20	5	0,0	0,0	5,0
Remanufactured	Control	Wand assembly	Wand Mechanism	3D printing	2	PLA	0,05	Kg	New	20	40	10,0	0,5	40,5
	Moulds	Foils	Main Vertical	Machining (CNC)	1,5	Aluminum	60,00	Kg	New	40	60	10,0	600,0	660,0
Remanufactured	Moulds	Foils	Orizzontal Main	Machining (CNC)	1	Aluminum	17,00	Kg	Upcycled	40	40	0,0	0,0	40,0
	Moulds	Foils	Orizzontal Rudder	Machining (CNC)	0,5	Aluminum	10,00	Kg	Upcycled	40	20	0,0	0,0	20,0
	Moulds	Foils	Vertical Rudder	Machining (CNC)	1,5	Aluminum	125,00	Kg	New	40	60	10,0	1250,0	1310,0
	Moulds	Hull	Campling			Wood Others	16,61	Kg	New	0	0	0,0	0,0	0,0
	Moulds	Hull	Deck	Machining (CNC)	5	Wood Others	41,29	Kg	New	40	200	0,0	0,0	200,0
New part	Moulds	Hull	Fairing	3D printing	45	ABS	20,00	Kg	New	20	900	50,0	1000,0	1900,0
	Moulds	Hull	Hull Shell			Glebanite	61,45	Kg	Upcycled	0	0	0,0	0,0	0,0
	Moulds	Hull	Keel Box	Machining (CNC)	2	Aluminum	12,00	Kg	New	40	80	10,0	120,0	200,0
	Rig	Adjustment	Cunningham			16 Single Hook	2,00	pz.	New	0	0	39,8	79,6	79,6
	Rig	Adjustment	Cunningham			Fly 18 Double	2,00	pz.	New	0	0	49,6	99,3	99,3
	Rig	Adjustment	Cunningham			Fly 18 Single	3,00	pz.	New	0	0	28,8	86,4	86,4
Remanufactured	Rig	Adjustment	Cunningham			Power sprint 78/ (TD99)	36,00	mt.	New	0	0	3,3	117,9	117,9
	Rig	Adjustment	Main			40 T2 Ratchamatic	1,00	pz.	New	0	0	85,5	85,5	85,5
	Rig	Adjustment	Main			40 Zircon Singke Beckert	1,00	pz.	New	0	0	76,1	76,1	76,1
	Rig	Adjustment	Main			40 Zircon Single	2,00	pz.	New	0	0	73,6	147,2	147,2
Remanufactured	Rig	Adjustment	Main			Olimpicstar 78	8,00	mt.	New	0	0	2,3	18,5	18,5
	Rig	Adjustment	Organizer			Calza Dsk coated	8,00	mt.	New	0	0	4,6	36,8	36,8
New part	Rig	Adjustment	Organizer			Carbo-Cam Micro	9,00	pz.	New	0	0	39,6	356,4	356,4
Remanufactured	Rig	Adjustment	Organizer			Dsk 78 ultra	20,00	mt.	New	0	0	2,8	56,4	56,4
Remanufactured	Rig	Adjustment	Organizer			Dsk 78 ultra	25,00	mt.	New	0	0	4,4	109,7	109,7
	Rig	Adjustment	Organizer			Guida Carbo-Cam Micro	6,00	pz.	New	0	0	10,4	62,3	62,3
	Rig	Adjustment	Organizer			Micro bullseye fairlead	6,00	pz.	New	0	0	5,9	35,6	35,6
	Rig	Adjustment	Organizer			Pulley	6,00	pz.	New	0	0	6,4	38,4	38,4
New part	Rig	Adjustment	Organizer			16mm sheave	20,00	pz.	New	0	0	11,6	232,0	232,0
New part	Rig	Adjustment	Organizer			29mm sheave	10,00	pz.	New	0	0	12,9	129,3	129,3
New part	Rig	Adjustment	Organizer			cheek air block	6,00	pz.	New	0	0	18,7	112,3	112,3
Remanufactured	Rig	Adjustment	Organizer			Treccia Dyneema	15,00	mt.	New	0	0	2,1	31,8	31,8
New part	Rig	Adjustment	Organizer			16mm High Load Cheek Block	4,00	pz.	New	0	0	53,9	215,4	215,4
	Rig	Adjustment	Vang			Fly 18 Double	1,00	pz.	New	0	0	49,6	49,6	49,6
	Rig	Adjustment	Vang			Fly 18 Single	2,00	pz.	New	0	0	28,8	57,6	57,6
	Rig	Adjustment	Vang			Fly 18 Triple	1,00	pz.	New	0	0	52,0	52,0	52,0
	Rig	Adjustment	Vang			Fly 29	2,00	pz.	New	0	0	149,8	299,5	299,5
	Rig	Boom	Boom			From a 2014 Mach2			Upcycled	0	0	0,0	0,0	0,0
	Rig	Must	Mast			From a 2013 Mach2			Upcycled	0	0	0,0	0,0	0,0
	Rig	Sail	Sail			4T Forte Recycled	8,25	sqm.	New	0	0	0,0	0,0	0,0
	Rig	Spreaders	Spreaders	Autoclave cure	4	Aluminum	0,05	Kg	New	40	160	10,0	0,5	160,5
	Rig	Spreaders	Spreaders			CF/Epoxy Prepreg Epoxy / Int Modulus CF (i.e T800)	0,30	Kg	New	0	0	400,0	120,0	120,0
	Rig	Spreaders	Spreaders			PET Recycled	0,10	Kg	New	0	0	0,0	0,0	0,0
	Rig	Deck	Pulley plates			CF/Epoxy Prepreg Epoxy / Std Modulus CF (i.e. T700)	0,10	kg	Upcycled	0	0	0,0	0,0	0,0
Remanufactured	Structures	Foils	Keel	Autoclave cure	With sprea	CF/Epoxy Prepreg Epoxy / Int Modulus CF (i.e T800)	1,24	Kg	New	40	0	400,0	496,0	496,0
Remanufactured	Structures	Foils	Keel			Dry fabric aramid Fibers Kevlar	0,05	Kg	Out of shelf life	0	0	60,0	3,0	3,0
Remanufactured	Structures	Foils	Keel			Dry fabric glass fibers S Glass	0,75	Kg	Out of shelf life	0	0	37,5	28,1	28,1
Remanufactured	Structures	Foils	Keel			Std. Epoxy Lamination Resin	0,49	Kg	Out of shelf life	0	0	12,5	6,1	6,1
Remanufactured	Structures	Foils	Rudder	Autoclave cure	(4) With s	CF/Epoxy Prepreg Epoxy / Int Modulus CF (i.e T800)	1,53	Kg	New	40	0	400,0	612,0	612,0
Remanufactured	Structures	Foils	Rudder			Dry fabric aramid Fibers Kevlar	0,05	Kg	Out of shelf life	0	0	60,0	3,0	3,0
Remanufactured	Structures	Foils	Rudder			Dry fabric glass fibers S Glass	0,93	Kg	Out of shelf life	0	0	37,5	34,9	34,9
Remanufactured	Structures	Foils	Rudder			Std. Epoxy Lamination Resin	0,60	Kg	Out of shelf life	0	0	12,5	7,5	7,5
New part	Structures	Foils	Rudder Bulb	Machining (CNC)	8	Stainless Steel	0,21	Kg	New	40	320	30,0	6,3	326,3
New part	Structures	Gantry	Gantry Type 1	3D printing	12	PETG	0,70	Kg	New	20	240	15,0	10,5	250,5
New part	Structures	Gantry	Gantry Type 1			Dry fabric Basalt Fibers	0,33	Kg	New	0	0	0,0	0,0	0,0
New part	Structures	Gantry	Gantry Type 1			Bio-Based Epoxy Lamination	0,12	Kg	New	0	0	15,0	1,8	1,8
New part	Structures	Gantry	Gantry Type 2			MMA Bonding	1,92	Kg	Out of shelf life	0	0	7,5	14,4	14,4
New part	Structures	Gantry	Gantry Type 2			Dry fabric Basalt Fibers	0,35	Kg	New	0	0	0,0	0,0	0,0
New part	Structures	Gantry	Gantry Type 2			PET Recycled	1,00	Kg	New	0	0	0,0	0,0	0,0
New part	Structures	Hull	Deck			Dry fabric Basalt Fibers	0,70	Kg	New	0	0	0,0	0,0	0,0
New part	Structures	Hull	Deck			MMA Bonding	2,18	Kg	New	0	0	15,0	32,7	32,7
New part	Structures	Hull	Deck			PET Recycled	0,57	Kg	New	0	0	0,0	0,0	0,0
New part	Structures	Hull	Fairing			Dry fabric Basalt Fibers	0,40	Kg	New	0	0	0,0	0,0	0,0
New part	Structures	Hull	Fairing			MMA Bonding	0,15	kg	Out of shelf life	0	0	7,5	1,1	1,1
	Structures	Hull	Fairing Bulkhead			Dry fabric Basalt Fibers	0,23	Kg	New	0	0	0,0	0,0	0,0
	Structures	Hull	Fairing Bulkhead			MMA Bonding	0,68	Kg	New	0	0	15,0	10,2	10,2
	Structures	Hull	Fairing Bulkhead			PET Recycled	0,09	Kg	New	0	0	0,0	0,0	0,0
	Structures	Hull	Hull Shell			Dry fabric Basalt Fibers	2,23	Kg	New	0	0	0,0	0,0	0,0
	Structures	Hull	Hull Shell			MMA Bonding	3,00	Kg	New	0	0	15,0	45,0	45,0
	Structures	Hull	Hull Shell			PET Recycled	0,74	Kg	New	0	0	0,0	0,0	0,0
	Structures	Hull	Keel Box			Dry fabric Basalt Fibers	0,21	Kg	New	0	0	0,0	0,0	0,0
	Structures	Hull	Keel Box			MMA Bonding	0,24	Kg	New	0	0	15,0	3,6	3,6
	Structures	Hull	Keel Box			PET Recycled	0,05	Kg	New	0	0	0,0	0,0	0,0
	Structures	Hull	Keel Box Bulkhead			Dry fabric Basalt Fibers	0,04	Kg	New	0	0	0,0	0,0	0,0
	Structures	Hull	Keel Box Bulkhead			MMA Bonding	0,12	Kg	New	0	0	15,0	1,8	1,8
	Structures	Hull	Keel Box Bulkhead			PET Recycled	0,02	Kg	New	0	0	0,0	0,0	0,0
	Structures	Hull	Mast Base			Carbon tubes	0,20	Kg	Upcycled	0	0	0,0	0,0	0,0
	Structures	Hull	Mast Base Bulkhead			Dry fabric Basalt Fibers	0,15	Kg	New	0	0	0,0	0,0	0,0
	Structures	Hull	Mast Base Bulkhead			MMA Bonding	0,45	Kg	New	0	0	15,0	6,8	6,8
	Structures	Hull	Mast Base Bulkhead			PET Recycled	0,06	Kg	New	0	0	0,0	0,0	0,0
	Structures	Hull	Transom			Dry fabric Basalt Fibers	0,96	Kg	New	0	0	0,0	0,0	0,0
	Structures	Hull	Transom			MMA Bonding	2,82	Kg	New	0	0	15,0	42,3	42,3
	Structures	Hull	Transom			PET Recycled	0,37	Kg	New	0	0	0,0	0,0	0,0
	Structures	Hull	Wings Stern Bulkhead			Dry fabric Basalt Fibers	0,06	Kg	New	0	0	0,0	0,0	0,0
	Structures	Hull	Wings Stern Bulkhead			MMA Bonding	0,16	Kg	New	0	0	15,0	2,4	2,4
	Structures	Hull	Wings Stern Bulkhead			PET Recycled	0,02	Kg	New	0	0	0,0	0,0	0,0
New part	Structures	Wings	Trampolines			PET Recycled	0,80	Kg	New	20	0	0,0	0,0	0,0
New part	Structures	Wings	Trampolines			Dry fabric Basalt Fibers	3,60	Kg	New	0	0	0,0	0,0	0,0
New part	Structures	Wings	Trampolines			MMA Bonding	4,40	Kg	Out of shelf life	0	0	7,5	33,0	33,0
New part	Structures	Wings	Cross Bars			PET Recycled	2,80	Kg	New	20	0	0,0	0,0	0,0
New part	Structures	Wings	Cross Bars			Dry fabric Basalt Fibers	1,60	Kg	New	0	0	0,0	0,0	0,0
New part	Structures	Wings	Cross Bars			MMA Bonding	0,85	Kg	Out of shelf life	0	0	7,5	6,4	6,4

Figure 2.7: Complete manufacturing data report (Higher expenses are highlighted in red)

3 SUSTAINABILITY ANALYSIS

3.1 General Description

Sustainability is one of the main pillars of the SuMoth Challenge and a guiding principle in the design of the Febe refit. The team strongly believes that structural reliability and weight reduction goals for the upgraded components must always be coupled with the goal of building a more sustainable SuMoth concept. The only right way to achieve this purpose is by quantifying the environmental impact of Febe's new components, which can be done by performing a life-cycle assessment (LCA). The MarineShift360 LCA tool, designed specifically for the marine industry, helped the team in this work. The collection of real data, and the research work on literature when real data were not available, allowed us to obtain a correct and accurate estimation of the environmental impact of the boat. The updated elements, for which an LCA was performed, are: Deck, Wings (composed by Trampolines and Crossbars), Gantry (type I and type II), Fairing, Rudder Bulb, Rudder Foil, Main Foil, and Hull Wrap.

3.2 Boat and Elements Lifecycle

For this year's competition, the team decided to preserve the hull of Febe to optimize other complementary parts in terms of performance, structural reliability, and, last but not least, sustainability. A notable example is the upgraded wings, designed to be completely made of recyclable materials like woven and unidirectional fabrics of basalt (FILAVA^{TM} by Isomatex S.A.) and thermoplastic resin for infusion processes (HELIUM by Arkema). Thanks to a pyrolysis process (a thermochemical process), original materials can be potentially recovered. Moreover, the choice of producing wings in two components (Trampolines and Crossbars) allows us to infuse them without any moulds. This is a natural step forward, in terms of sustainability, from the previous version of Febe's wings, which were produced with pre-preg carbon fiber and glass fiber sheets (a post cure in oven was needed) and by using various moulds for longitudinal/transversal tubes and joints. When it's not possible to avoid the use of moulds (as with the fairing), they are designed to be 3D printed: this process allows us to create complex-shaped parts without huge energy loss and with little material waste. Lastly, Febe's old deck was cut and shaped to realize new bulkheads, giving new life to obsolete components and respecting the zero-waste approach.

3.3 Actions for a Sustainable Future

Increasing environmental and sustainability awareness has driven research into innovative methods to reduce human-made pollution. The key lies in adopting more sustainable processes and methods, as well as never slow down on the research of new, more sustainable materials, even if the one currently used ones reach unique performance to sustainability ratios.There is no definitive solution to a more sustainable future, it's built from the bottom up, step by step and trough constant change. One of the most effective ways to minimize human-made pollution is to prioritize the use of second-hand materials over new ones and emphasizing the importance of recyclable materials. In the realm of composites,materials such as thermoplastic resins and basalt fibers,that could potentially be remelted and reshaped, play a critical role in components recyclability. Production methods and processes also have a big impact on the human ecological footprint; sustainable manufacturing must be taken into consideration as a major focus. The design is a fundamental part of the manufacturing process; in fact, it allows to minimize material usage and evaluate waste,cost impact,and environmental outcome. From this perspective, approaches such as Life cycle assessments, that are aimed to evaluate the impact on the environment of a product during all steps of the production till the end of life, are becoming more and more important even in the early design phase to take

quantitative steps towards true sustainability. For us future engineers, the SuMoth Challenge is a test field to study, experiment, and work concretely on new ideas to achieve a sustainable design, which lays on the concept of realizing an object by enhancing its longevity and durability rather than just building a "single use product". The boats our team built, Teti and Febe, are excellent examples of sustainable design. Both Teti, which was built two years ago, and Febe, which was built last year, have been improved and fixed rather than being replaced with new ones built from the bottom up. In conclusion, seeing how much human waste and pollution is affecting our planet, we deem it necessary to find new methods and processes to work with eco-friendly materials. These are the goals that our team has set, and through the SuMoth Challenge, we are trying to bring our ideas to life to contribute to building a better and cleaner future for the manufacturing industry.

4 TEAM

4.1 Team Members

This year, the team has undergone a significant generational shift. Many longstanding members have completed their university studies and embarked on new careers. Drawing on their experience within the Polimi Sailing Team, many have secured jobs in the nautical and manufacturing sectors. Leadership of the team has transitioned to a new group of leaders, while the team itself has welcomed a significant number of new members. Specifically, the total number of members has reached 92, and female participation has increased proportionally to the total membership.

	Women	**Men**	**Total**
Absolute	13	79	92
Percentage	14%	86%	100%

Table 4.1: Team members

4.2 Acknowledgements

The PoliMi Sailing Team wants to extend its heartfelt gratitude to the numerous individuals and organizations whose unwavering support has been essential to our accomplishments. Firstly, we sincerely thank the Politecnico di Milano for their invaluable support. In particular, we acknowledge the Department of Design for their steadfast assistance in navigating complex administrative processes. Their help has been crucial in ensuring our project's smooth progress. We are profoundly grateful to Professors Arianna Bionda and Andrea Ratti for their consistent support and patience throughout this challenging season. Their mentorship and guidance have been key to shaping our team's approach and success. We also extend our deep appreciation to our sponsors for their generous contributions, which have been critical in helping us achieve our project goals. Their belief in our mission and commitment to fostering innovation and sustainability are greatly valued. The SuMoth Challenge has provided an extraordinary opportunity for us to compete and collaborate with distinguished universities and outstanding projects. This experience has not only built meaningful connections but also motivated us to push the limits of innovation while maintaining a strong emphasis on sustainability. Lastly, we express our utmost appreciation to every member of the PoliMi Sailing Team. Their unwavering dedication, resilience, and collective efforts have enabled us to overcome obstacles and make remarkable progress. Their passion for creating a sustainable future is truly inspiring. In conclusion, the PoliMi Sailing Team sincerely thanks everyone who has supported us along this journey. Your contributions, no matter how big or small, have significantly impacted our project's success. Together, we are working towards a brighter and more sustainable future.

4.3 Sponsors

The technical and financial support from our partners enables us to continue researching innovative techniques for more efficient and sustainable design and production in the nautical and composite materials sectors. This year, the team has focused on strengthening and expanding its partnerships, bringing the total number of collaborating companies to 34.
We are deeply grateful to all the companies and organizations that have believed in our project over the years and have generously offered their support.

Figure 4.1: 2024 Partners

5 MARINESHIFT 360 LCA

The Polimi Sailing Team strongly believes in the importance of the sustainability aspect of its vessels. For this purpose, a Life Cycle Assessment (LCA) of Febe, our entering SuMoth for the 2024 Foiling SuMoth Challenge, was conducted. LCA is an objective method of understanding what the environmental footprint of a product will be over its full life cycle, from cradle to grave, regulated by the international standards ISO 14040 [10]. Febe was realized last year to participate in the 2023 Foiling SuMoth Challenge. Reused components without any sizing or changes (e.g., hull, sail, foils' aluminum moulds, etc.) are not assessed in this LCA. Only new components are assessed in this LCA, and they are the following:

- Deck
- Wings (composed by Crossbars & Trampolines)
- Fairing
- Gantry (Type 1)
- Gantry (Type 2)
- Rudder Bulb
- Rudder Foil
- Main Foil
- Hull Wrap

According to the competition's rules, this sustainability analysis was performed using MarineShift360 software (MS360) [12] for data entry and life cycle analysis. The MS360 LCA tool is a purpose-built tool designed by marine industry experts for the marine sector. MS360 calculates the environmental impact across 8 impact categories:

- Global warming potential (fossil & non-fossil – expressed in $kgCO_2e$)
- Material resource scarcity (expressed in *kgCue*)
- Energy consumption (non-renewable & renewable – expressed in *MJ*)
- Water consumption (expressed in m^3)
- Marine eutrophication (expressed in *kgNe*)
- Waste factor (expressed as a percentage)

Whenever it was possible, data related to the actual quantities of materials used during the manufacturing phase were recorded and collected. When this was not feasible (data difficult to find, or referring to components still in the design phase), estimations were made as best as possible by looking at the nominal dimensions of the components and the technical datasheet of the fabrics. The system boundary includes material quantities (ordered & final) involved in the manufacturing processes, energy use, downstream transport of the final part from the shipyard in Dervio (LC) to Malcesine (assessed with the "Use phase - Passenger" template provided by MS360). This study excludes the upstream transport of the single raw materials and material quantities relating to mechatronic components (as they are difficult to find and usually not so precise). For what concerns the End of Life (EoL) of boat's components, it is important to underline that all of them were designed to be reused in the making of new SuMoth concepts for next years' competitions. Moreover, some components (like the wings and the gantry) were redesigned to be completely made of sustainable materials, thanks to the use of a thermoplastic infusion resin that can be potentially "remelted," allowing us to recover fiber fabrics to reuse for new infusion in the next challenge. The team will surely research this topic in the future, with the hope to implement this solution in the following seasons.

5.1 Results

In the following Table 5.1, the numerical results of the different impact categories provided by MarineShift360 are shown.

FINAL RESULTS		
Global warming - fossil	650.25	$kgCO_2e$
Global warming - non-fossil	18.59	$kgCO_2e$
Mineral resource scarcity	2.61	$kgCue$
Energy consumption - non-renewable	12370	MJ
Energy consumption - renewable	716.26	MJ
Water consumption	6.39	m^3
Marine eutrophication	0.05	$kgNe$
Waste factor	35.32	%

Numerical values of the 8 impact categories

Table 5.1: table

In Figure 5.1 and 5.2, the global warming potential (GWP) of the making of a material (or a specific process) is illustrated. It represents the effect of the increasing level of greenhouse gases on the atmosphere's temperature. In Figure 5.1, the biggest value (almost 20%) comes from the transport phase, which, however, does not provide any contribution in Figure 5.2, due to the fossil nature of fuels.

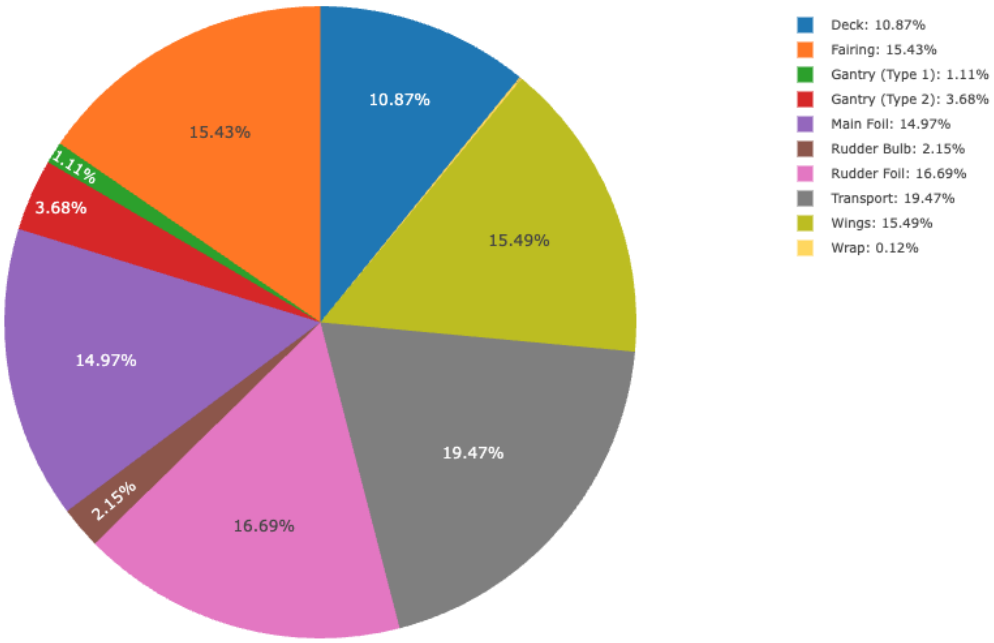

Figure 5.1: Global warming potential - Fossil

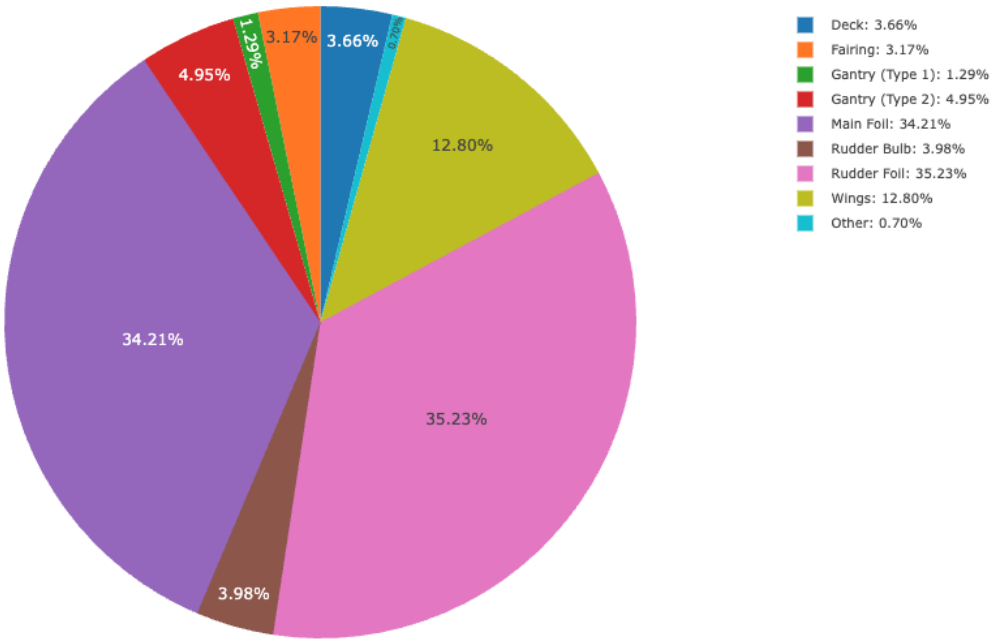

Figure 5.2: Global warming potential - Non-fossil

In Figure 5.3, the mineral resource scarcity is illustrated. It represents the extraction of minerals on available reserves. The biggest contribution comes from the rudder bulb, caused by the use of steel in its production, followed by the transport phase (high values due to the extraction of fossil fuels).

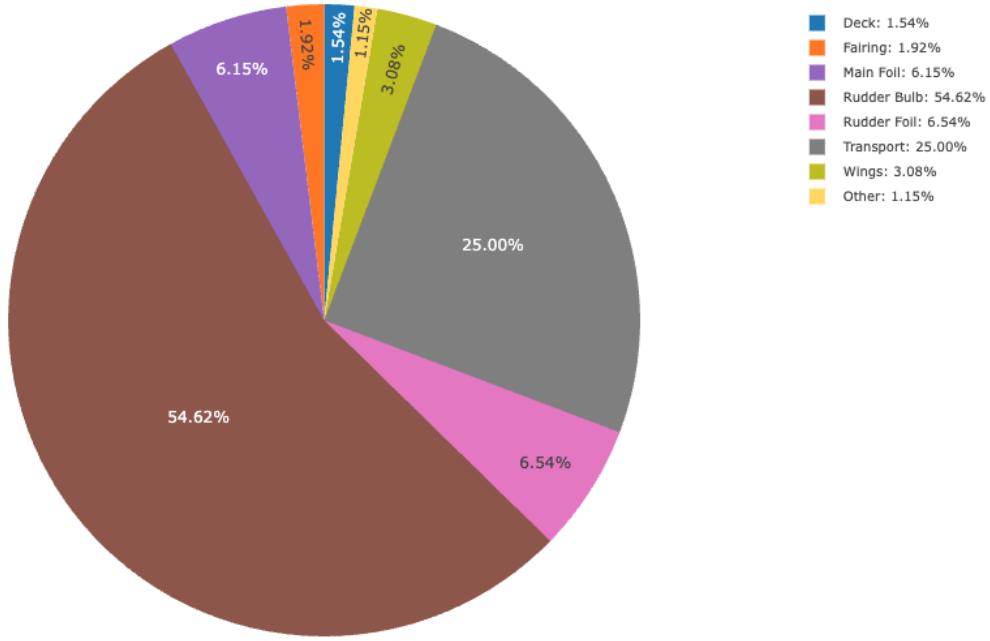

Figure 5.3: Mineral resource scarcity

In Figure 5.4 and 5.5, the energy consumption is shown. It represents the total quantity of energy harvested from non-renewable and renewable resources from nature, respectively. The driving parameter is the manufacturing process used: the largest values come from the foils (autoclave curing process), followed by the fairing (fairing mould was 3D printed). Both gantries

don't exceed 5%, mainly thanks to the fact that they are designed to be hand laminated.

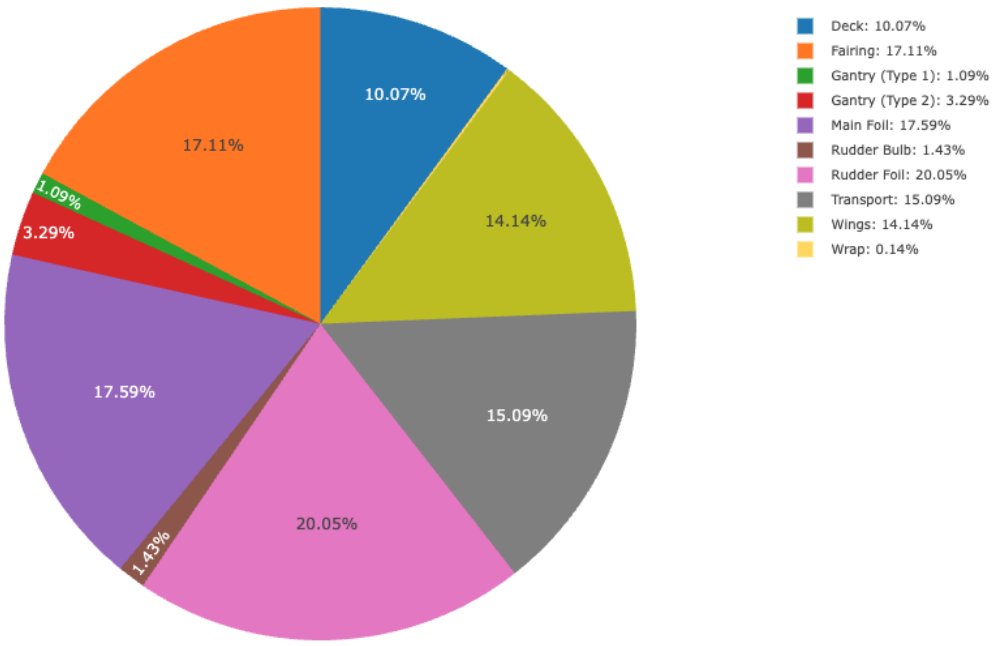

Figure 5.4: Energy consumption - Non-renewable

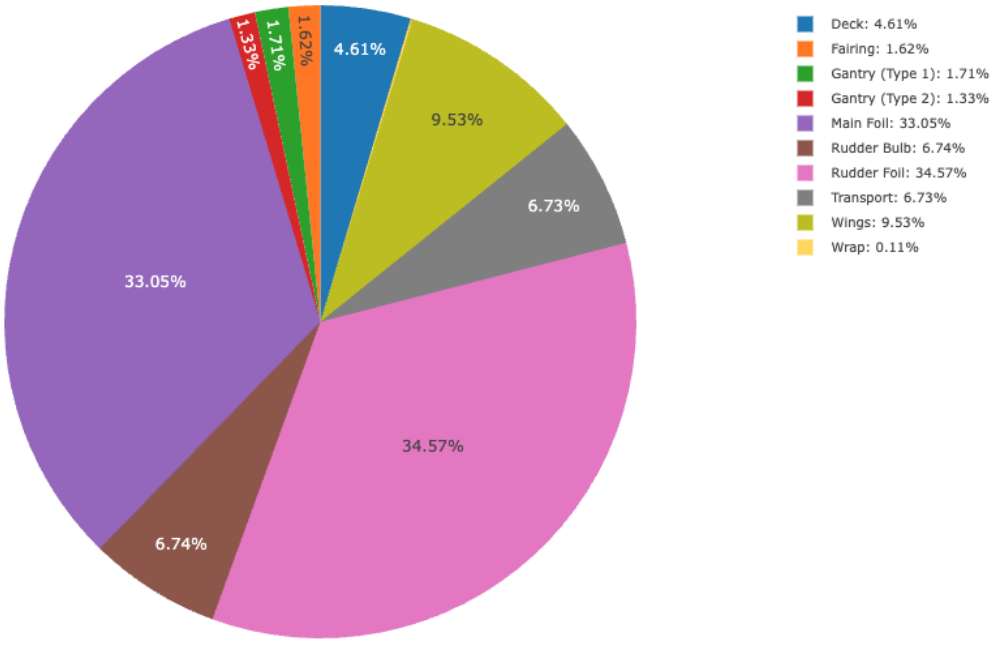

Figure 5.5: Energy consumption - Renewable

In Figure 5.6 and 5.7, the water consumption and marine eutrophication of the production are illustrated. The water consumption represents the total quantity of water (expressed in m^3) for the making of the materials. The largest slices come from the foils (realized with pre-preg sheets) and the fairing (from ABS granulate with which its mould was produced).

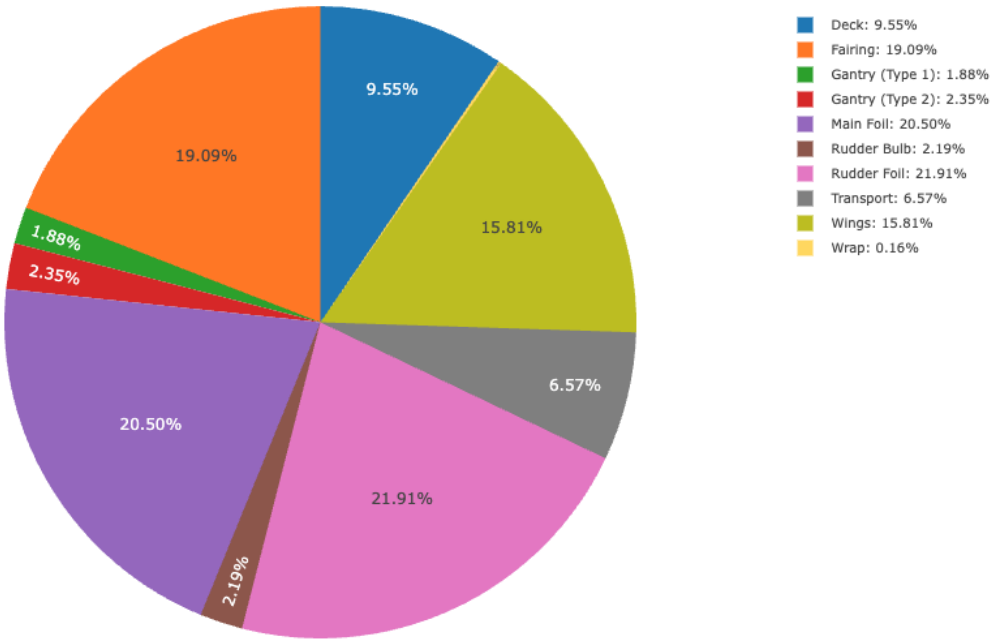

Figure 5.6: Water consumption

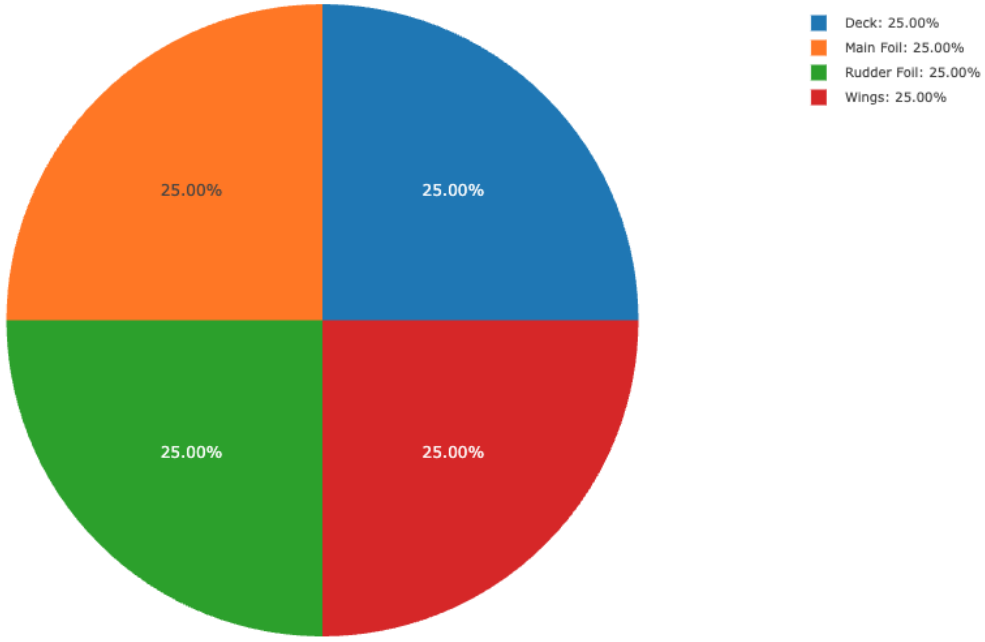

Figure 5.7: Marine eutrophication

Lastly, in Figure 5.8, the waste factor, which represents the weight ratio of (ordered + auxiliary - final material)/(ordered + auxiliary material), is shown. The higher values come from the wings (realized in 3 distinct vacuum infusion processes) and from the rudder bulb (milled from a full block of stainless steel). For all the components, several nesting scenarios were studied to minimize the waste materials directly in the design phase. This LCA doesn't take into account that some auxiliary materials involved during infusions can be reused (resulting in an overestimation of real values).

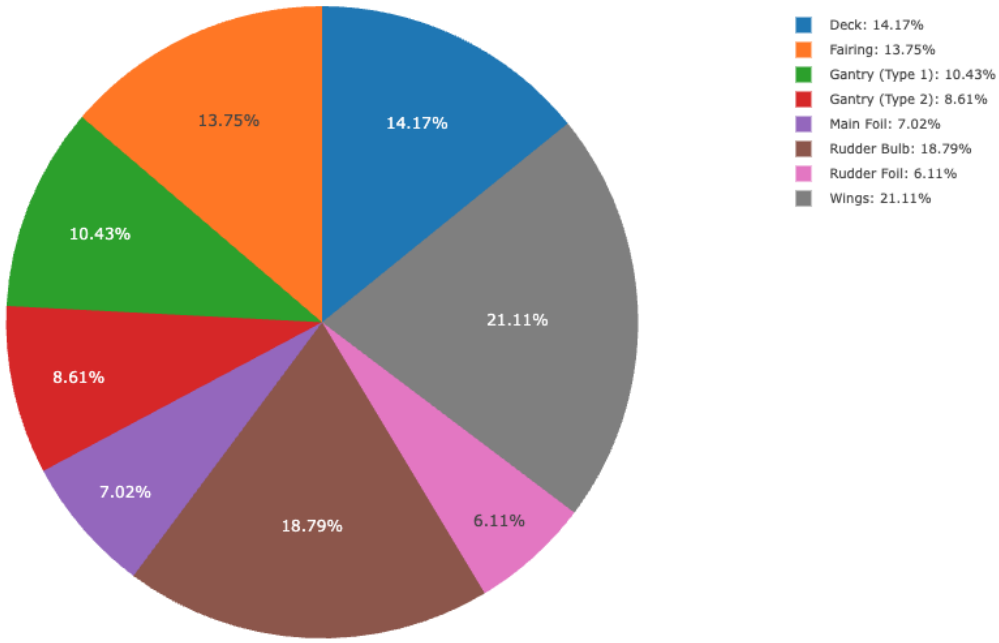

Figure 5.8: Waste factor

5.2 Comparison Between Old and New Wings

A great deal of work was done in the design phase of the new wings. The choice to make them with an infusion process by using dry basalt fibre fabrics and thermoplastic resin allowed us to completely avoid pre-preg carbon and glass fibre sheets. Furthermore, no moulds were necessary, thanks to the idea of dividing the wings into two components (Trampolines and Crossbars) instead of making them in a single skeleton. For these two aspects, it is interesting to make a comparison between the new and old wings in terms of the 8 impact categories to see if there have been improvements concerning their sustainability.

	Old Wings	New Wings	Percentage change
Global warming - fossil ($kgCO_2e$)	280.51	100.74	-64%
Global warming - non-fossil ($kgCO_2e$)	12.64	2.38	-81%
Mineral resource scarcity ($kgCue$)	1.21	0.08	-93%
Energy consumption - non-renewable (MJ)	5893	1749	-70%
Energy consumption - renewable (MJ)	602	68.24	-89%
Water consumption (m^3)	3.59	1.01	-72%
Marine eutrophication ($kgNe$)	0.03	0.01	-67%
Waste factor (%)	27.62	36	+30%

Sustainability comparison between the old and new wings

Table 5.2: table

In Table 5.2, it's possible to see notable improvements in terms of sustainability along all the impact categories. The only exception comes from the waste factor, where there was a small increase from the last version, but as already stated before, this value is overestimated (by not taking care of auxiliary materials' reuse involved in all the infusion processes).

Bibliography

[1] John Anderson. *Fundamentals of Aerodynamics*. 2016. ISBN: 978-1259129919.

[2] National Marine Electronics Association. *NMEA - National Marine Electronics Association*. https://www.nmea.org/.

[3] CIT Composite Italian Toray. *CIT Composite Italian Toray: Advanced Composite Materials*. Provided technical and material support for the project. 2024. URL: https://www.citcomposites.it.

[4] Microsoft Corporation. *Microsoft Excel*. https://www.microsoft.com/en-us/microsoft-365/excel. Accessed: 2024-05-20. 2024.

[5] Diab. *Sponsorship Support*. Provided financial and technical support for the project. 2024.

[6] Eligio Re Fraschini. *Eligio Re Fraschini: Innovative Solutions for Industry*. Provided technical and financial support for the project. 2024. URL: https://www.eligio.it.

[7] Open Source Robotics Foundation. *ROS - Robot Operating System*. https://wiki.ros.org/.

[8] Gottifredi Maffioli. *Company Overview*. http://www.gottifredimaffioli.com. [Online; accessed 20-May-2024]. 2024.

[9] Harken. *Product Catalog*. http://www.harken.com. [Online; accessed 20-May-2024]. 2024.

[10] International Organization for Standardization. *Environmental Management - Life Cycle Assessment - Principles and Framework*. ISO 14040:2006. ISO. Geneva, Switzerland, 2006. URL: https://www.iso.org/standard/.

[11] International Organization for Standardization. *ISO 11898-2:2024 Road vehicles – Controller area network (CAN)*. Geneva, Switzerland: International Organization for Standardization, 2024.

[12] *Marine Shift 360*. Accessed: 2024-05-20. 2024.

[13] OpenFOAM Foundation. *OpenFOAM+: The Open Source CFD Toolbox*. https://www.openfoam.com/. Version 10, Accessed: 2024-05-14. 2024.

[14] Odoo S.A. *Odoo*. https://www.odoo.com. Accessed: 2024-05-20. 2024.

[15] SmartCAE. *SmartCAE: Advanced Simulation Software*. Version 5.0. 2024. URL: https://www.smartcae.com.

[16] Dassault Systèmes. *Abaqus*. https://www.3ds.com/products-services/simulia/products/abaqus/. Accessed: 2024-05-20. 2024.

[17] The MathWorks Inc. *MATLAB: The Language of Technical Computing*. Version R2023b. The MathWorks Inc. Natick, Massachusetts, 2024. URL: https://www.mathworks.com/products/matlab.html.

[18] WASP 3D. *WASP 3D: High-performance 3D Printing Solutions*. Version 3.0. 2024. URL: https://www.wasproject.it.

Appendix A - Engineering and Design

A.1 Foil optimisation

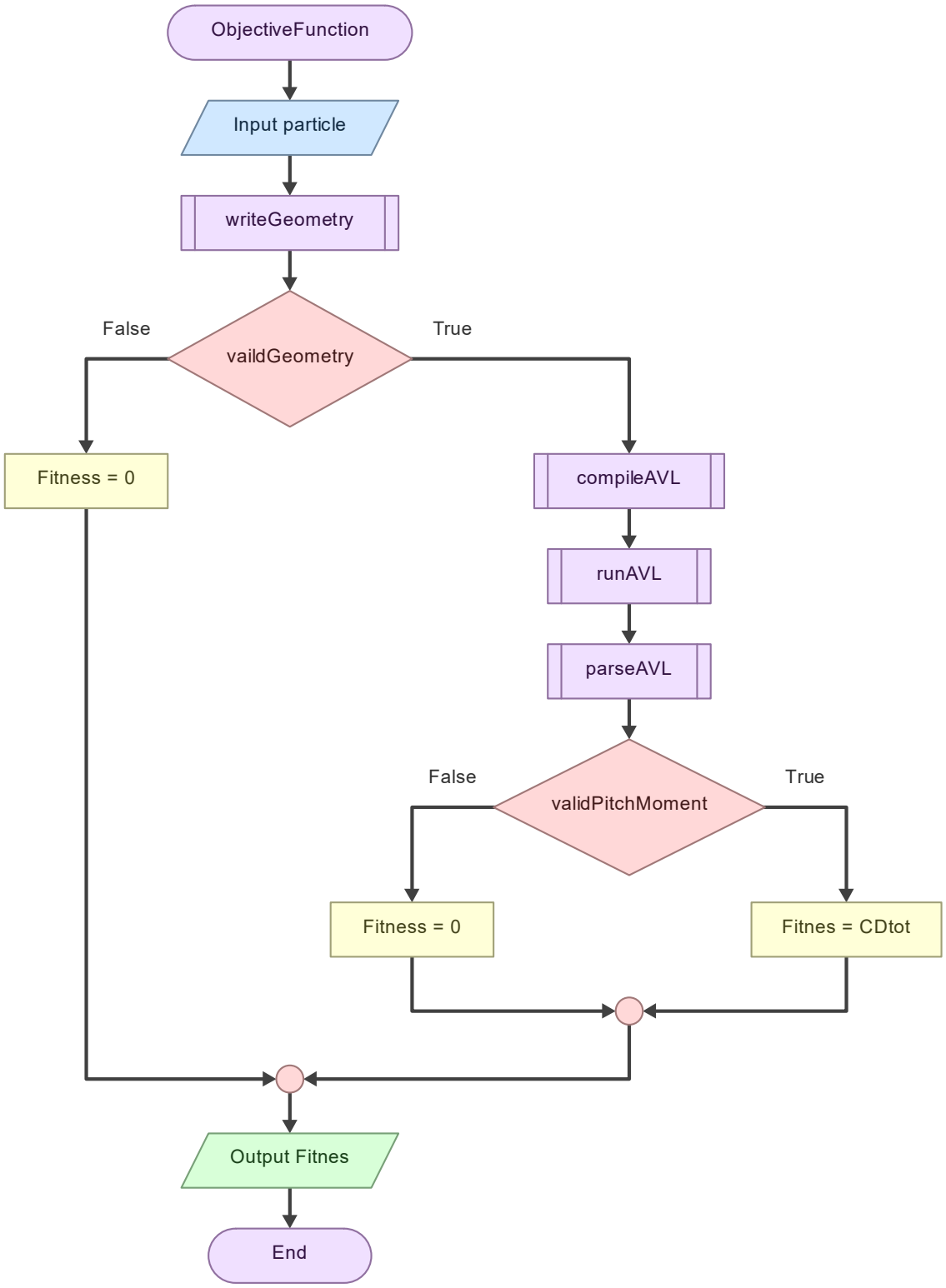

Figure 9: Objective function

A.1.1 Low Fidelity Optimization

To optimise the shape of Moth's foil we resort, in preliminary analysis, to the use of quickly operating genetic algorithms written in Matlab [17]. The code was rewritten entirely, following a heavy rethought process that successfully tackled problems encountered in previous years. The solver we chose is Athena Vortex Lattice (AVL), which implements a Vortex Lattice Method (VLM). In the following chapter we will present firstly how the solver works and secondly how we implemented the optimization process.

A.1.2 Kutta-Joukowski Condition:

A VLM uses the following hypothesis to simulate the flow:

- Incompressible flow
- Irrotational flow
- Inviscid flow
- Small attack angle

Assured that the previous conditions are met, via the Kutta-Joukowski theorem we can assume that for a large Reynolds number, the fluid has an inviscid flow even at the boundary layer, which in reality is a viscous region (as proved by Prandtl). For our sailing condition we can estimate the Reynolds number to be above 1'000'000. Also, we estimate that the angle of attack alpha between the water flow and the foil is at maximum 2-3°, meeting the previous requirements. This allows it to work with potential flow theory and horseshoe vortices, which are some of the main characteristics of the VLM. Since these criteria are met, the Kutta-Joukowski theorem allows us to calculate the lift of a foiling surface known its speed, the density of the fluid and its circulation around the foil.

A.1.2.1 The Model

The Panel Method allows one to calculate numerically the solution of a given fluid dynamic problem on a three-dimensional surface as long as the velocity potential satisfies Laplace's equation. Using the B-spline method on curves, we can discretize a given geometry. Doing so, we can have points with different densities which represent and define each panel as the intersection of 4 splines with a collocation point in its middle. The surface boundary condition is evaluated at collocation points resulting in one equation to be solved for each collocation point. The formulation considered for the 3D panel method is zero trailing edge circulation that consists of two filaments: one belonging to the upper surface vortex panel, the other to the lower surface vortex panel. The circulation at the trailing edge is the difference of upper and lower panel circulation. This circulation can be cancelled by addition of a wake panel with the proper circulation, effectively imposing Kutta's condition.

Furthermore, each panel can be considered as a single horseshoe vortex. The horseshoe vortex consists of three segments: a bound vortex spanning the wing, connected to two trailing vortices at each wingtip. As required by the Kutta-Joukowski theorem, the circulation Γ is constant along the entire vortex line, and the vortex line extends downstream to infinity. Although this model qualitatively reproduces the observed tip vortices, it is not well suited for accurate prediction of overall wing lift and induced drag, which is its main weakness.

These techniques are advantageous because any flowfield of interest can be resolved by distributing singular functions over the body boundaries without the need of defining and solving a grid for the surrounding fluid domain. The computational effort is drastically reduced with respect to volume-based methods, at the same time that pretty accurate solutions can be achieved.

A.1.2.2 Vortice Lattice Method:

Following Anderson's [1] observations, thanks to the Kutta-Joukowski theorem, we're allowed to consider the flow field as a conservative vector field and express the fluid's velocity as the sum of the unperturbed fluid's velocity and the gradient of perturbation velocity potential:

$$v = v_\infty + \nabla\phi \tag{1}$$

The velocity potential ϕ satisfies Laplace's equation, allowing us to consider a complex flow as the superposition of elementary flow, which are also incompressible and irrotational.

As aforementioned, the lifting surfaces are divided into quadrilateral panels, each one with a corresponding horseshoe vortex (which serves the role of the elementary flow previously stated) and a collocation point. On each collocation point a normal vector is placed, so that it's normal to the camber surface. The vortex strength gamma is defined as the circulation of the fluid's velocity around the segments of the horseshoe vortices. Since lift is given by the pressure difference on the faces of each panel, a non null circulation implies a velocity differential between upper and lower flow, which via the Bernoulli principle induces the desired pressure differential.

The total perturbation velocity at a fixed collocation point is finally obtained by adding up the contributions of each horseshoe vortex that composes the foil's surface.

Given that the VLM neglects pressure and viscosity drag, a Neumann boundary condition is set, which prescribes that the normal velocity across the camber surface is zero. This flow tangency condition allowed us to previously consider the velocity as the sum of the freestream velocity and the perturbation velocity potential, since the normal velocity is supposed to be zero. By giving in input the Aerodynamic Influence Coefficient (AIC) matrix w_{ij} and simulation conditions, the Neumann condition is as follows:

$$v_i \cdot n_i = \left(v_\infty + \sum_{j=1}^{N} w_{ij}\Gamma_j \right) \cdot n_i = 0 \tag{2}$$

From this global condition, a system of N equations is obtained and then solved for all vortices strengths Γ_j.

On each panel acts a force with direction given by the vector product between the direction of propagation of the streamflow and the transverse segment l_i of the horseshoe vortex. The magnitude of the force is given by the previously mentioned Kutta-Joukowski formula (A.1.2):

$$F_i = \rho\Gamma_i(v_\infty + v_i) \wedge l_i \tag{3}$$

Being the force vector oriented in 3D space, we consider its components on three orthogonal axes for each panel, where the z axis is azimuthal and the y axis is aligned with the transverse segment of the panel. In the case of zero sideslip (freeflow stream velocity normal to the y axis) the only two resulting components are induced drag and lift, and they solely depend on the attack angle:

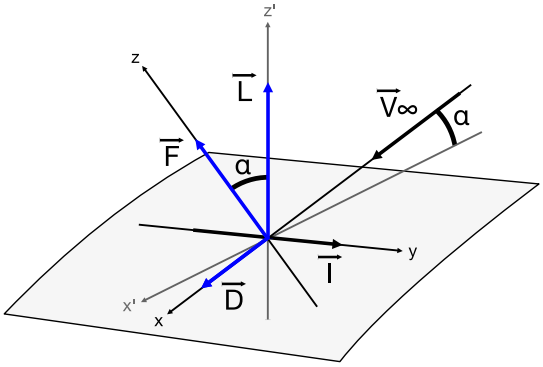

$$\begin{cases} D_i = F_x \cos\alpha + F_Z \sin\alpha \\ L = -F_x \sin\alpha + F_z \cos\alpha \end{cases} \tag{4}$$

Figure 10: Decomposition of the force acting on the panel

The total resultant force, lift and induced drag, are then obtained by adding each panel's contribution. This is qualitatively the way a VLM operates the calculations we then avail to optimise our foil design.

With an elliptical distribution configuration, the lift generated along the wing is proportional to the length of the wing span at each point along the wing itself. This implies that the lift is maximum near the centre of the wing and decreases uniformly toward the wingtips. With elliptical lift distribution the induced drag is minimised: this distribution produces more uniform airflow along the wing and reduces the formation of vortices at the wingtips. Wings with this configuration provide better aerodynamic efficiency and performance.

Appendix B - Team Members

Role	Name
Team Leader	Giorgio Panichi
Team Leader	Emanuele Galbiati

Table 3: Team Leaders

Role	Name
Head of department	Marco Furlani
Media Design Specialist	Maria Del Coro Karch Brosa
Public Relations Specialist	Chiara Rizzo
Logistics Planning Specialist	Sophie Ruth Sacerdote
Public Relations Campaign Manager	Vittoria Mariani
Logistics Planning Specialist	Andrea Abbondanza
Photographer	Francesco Redaelli
Public Relations Specialist	Federica Eoli
Social Media Manager	Marco Ferrari
Human Resources Specialist	Giorgia Marcucci
Media Design Specialist	Andrea Congiu

Table 4: Management & Communication Department

Role	Name
Head of department	Gianluca Grinovero
Control system specialist	Steven Horner
Team Leader	Giorgio Panichi
PCB Design	Alessia Maria Di Capua
Software developer	Gianluca Brambilla
CAD Designer	Francesco Valerio Persio Pennesi
OnBoard computer dev	Gabriele Caslini
PCB Design	Francesco Fioretti
Software developer	Samuele Calosso
Software developer	Tommaso Bocchietti
Software developer	Niccolò Giannone

Table 5: Mechatronics Department

Role	Name
CFD engineer	Alessandro Bellezza
Foil optimization	Zaccaria Ippoliti
Foil designer	Ludovico La Tora
Mathematic specialist	Chiara Nonino
Composite materials specialist	Matilde Danielli
CFD specialist	Michele Piffari
Driver and coach	Mattia Cislaghi
Terminato	Nicola Dell'Aera
Foil designer	Lorenzo Di Battista
Foil designer	Matteo Selden
Head of department	Marco Masala
Foil designer	Lorenzo Angelo Aloisi
CAD Designer	Luca Nordera
CFD specialist	Francesco Taddeo
Composite lamination expert	Federico Mistri

Table 6: Performance Department

Role	Name
Boat handler	Giacomo Bozzoli Parasacchi
Head of department	Giacomo Galbiati
Manufacturing Specialist	Federico Fersini
Rig designer	Federico D'Agostino
Boat handler and driver	Luis Fernando De Terry Soler
Skipper	Giovanni Masiero
Machining operator	Lorenzo Corradi
Sailing coach	Gianmarco Planchestainer
Team Leader	Emanuele Galbiati
Skipper	Pietro Caminiti

Table 7: Shore Team Department

Role	Name
2025 Project Coordinator	Francesco Rizzi
Head of Department	Niccolò Fantini
Rudder Designer	Lorenzo Macchioni
Rudder Designer	Federico Natali
Lca Specialist	Vincenzo Anania
Vice-Head of Department	Francesco Greco
Vice-Head of Department	Pietro Formenti
Rudder Fem Analyst	Diego Giampiccolo
Manufacturing Operator	Niccolò Marino
Manufacturing Operator	Francesco Lunghi
Wing Fem Analyst	Martino Saraceno
Rudder Fem Analyst and Manufacturing Operator	Cesare Cassetti
Rudder Fem Analyst and Manufacturing Operator	Carlo Alberto Santini
Rudder Fem Analyst and Manufacturing Operator	Roberto Carrara
Rudder Fem Analyst and Manufacturing Operator	Alessandro De Paola
Structural Health Monitoring Designer	Riccardo Caliri
Rudder Designer	Francesco Tempestilli
Manufacturing Operator	Lorenzo Baldoni
Rudder Designer	Samuele Maria Giovanni Pampallona
Rudder Fem Analyst and Manufacturing operator	Alessandro Carella
Technical Director	Roberto Faure Ragani
Rudder Designer and Manufacturing operator	Bianca Spanedda
Wing Fem Analyst and Designer	Pietro Agostinacchio
Rudder Fem Analyst and Designer	Paolo Meda
Alumnus	Lorenzo Miele
Alumnus	Michele Vezzoli
Lca Specialist	Sara Sabatucci

Table 8: Structures Department